Scenarios of Global Change: Integrated Assessment of Climate Impacts

Sergey Paltsev, Andrei Sokolov, Henry Chen, Xiang Gao, Adam Schlosser, Erwan Monier, Charles Fant, Jeffery Scott, Qudsia Ejaz, Evan Couzo, Ronald Prinn and Martin Haigh

MIT JOINT PROGRAM ON THE SCIENCE AND POLICY of GLOBAL CHANGE

Report No. 291
February 2016

The MIT Joint Program on the Science and Policy of Global Change combines cutting-edge scientific research with independent policy analysis to provide a solid foundation for the public and private decisions needed to mitigate and adapt to unavoidable global environmental changes. Being data-driven, the Program uses extensive Earth system and economic data and models to produce quantitative analysis and predictions of the risks of climate change and the challenges of limiting human influence on the environment—essential knowledge for the international dialogue toward a global response to climate change.

To this end, the Program brings together an interdisciplinary group from two established MIT research centers: the Center for Global Change Science (CGCS) and the Center for Energy and Environmental Policy Research (CEEPR). These two centers—along with collaborators from the Marine Biology Laboratory (MBL) at Woods Hole and short- and long-term visitors—provide the united vision needed to solve global challenges.

At the heart of much of the Program's work lies MIT's Integrated Global System Model. Through this integrated model, the Program seeks to: discover new interactions among natural and human climate system components; objectively assess uncertainty in economic and climate projections; critically and quantitatively analyze environmental management and policy proposals; understand complex connections among the many forces that will shape our future; and improve methods to model, monitor and verify greenhouse gas emissions and climatic impacts.

This reprint is one of a series intended to communicate research results and improve public understanding of global environment and energy challenges, thereby contributing to informed debate about climate change and the economic and social implications of policy alternatives.

Ronald G. Prinn and John M. Reilly,
Program Co-Directors

For more information, contact the Program office:
MIT Joint Program on the Science and Policy of Global Change

Postal Address:
Massachusetts Institute of Technology
77 Massachusetts Avenue, E19-411
Cambridge, MA 02139 (USA)

Location:
Building E19, Room 411
400 Main Street, Cambridge

Access:
Tel: (617) 253-7492
Fax: (617) 253-9845
Email: ***globalchange@mit.edu***
Website: ***http://globalchange.mit.edu/***

Scenarios of Global Change: Integrated Assessment of Climate Impacts

Sergey Paltsev[*,†], Andrei Sokolov[*], Henry Chen[*], Xiang Gao[*], Adam Schlosser[*], Erwan Monier[*], Charles Fant[*], Jeffery Scott[*], Qudsia Ejaz[*], Evan Couzo[*], Ronald Prinn[*] and Martin Haigh[‡]

Abstract

Using the MIT Integrated Global System Modeling (IGSM) framework, we assess the climate impacts of emission scenarios exhibiting global mean surface temperatures ranging between 2.4°C and 4.3°C above pre-industrial by 2100. We compare the outcomes from these forward-looking scenarios against the common goal described by the target-driven scenario of 2°C. Without further policy measures, the agreement at COP-21 in Paris is projected to result in a 3.5°C increase in global temperature in 2100 relative to pre-industrial levels. Scenarios developed by Shell International (called Mountains *and* Oceans*) exhibit a substantial movement towards temperature stabilization, as they result in increases of only 2.4–2.7°C by 2100. Valuable components of these scenarios include a substantial shift to renewable energy and deployment of carbon capture and storage (CCS). These scenarios are successful in mitigating a large portion of water stress impacts and air pollution damages. They also significantly mitigate increases in ocean acidity. These projections show the significant value of policies that do not quite reach 2°C stabilization, but fall substantially close to that target by the end of the century. The challenge of meeting the Paris Agreement's aspiration to limit warming to 1.5°C is monumental, yet may be desirable if societies see the 2°C impacts, described here, as running too much risk.*

Contents

[*] MIT Joint Program on the Science and Policy of Global Change, Massachusetts Institute of Technology, MA, USA
[†] Corresponding Author (Email: paltsev@mit.edu)
[‡] Shell Scenarios Team, Shell International Ltd, London, UK

1. INTRODUCTION

There is a growing body of literature that tries to quantify the physical and economic impacts of future climate change (EC, 2014; EPA, 2015). Because the world has not experienced such high greenhouse gas (GHG) concentrations and temperatures in recent history, these assessments rely on modeling the human and climate systems, and they are subject to substantial uncertainty (Reilly *et al.*, 2013). Many impact assessments focus on a scenario of stabilization at 2°C above pre-industrial levels, a goal that the international community commonly sets as a target to reduce the negative impacts of climate change (IPCC, 2014). With the submission of the Intended Nationally Determined Contributions (INDCs) to the UN Framework Convention on Climate Change (UNFCCC) for the UN climate negotiations in Paris in December of 2015, it seems clear that global emissions will remain well above the pathways that the Intergovernmental Panel on Climate Change (IPCC) estimates would be consistent with achieving no more than 2°C temperature increase (Jacoby and Chen, 2014, 2015; MIT Joint Program, 2015).

The 1.5°C or 2°C goals can be analyzed using an exercise that involves working backwards and asking what must be done to achieve it. Another way is to devise scenarios that start from where we are now, then fit together policies that countries are currently proposing, examine how they might reasonably evolve in time, and incorporate possible trends in technology and energy use. Then these scenarios are analyzed to see where these take us in terms of future climate. We take this latter approach, and specifically examine two scenarios developed by the Shell Scenarios Team (Shell, 2013; data update from 2014 is used in this paper) that build on the current interest in carbon pricing systems and their increasing use as policy instruments of choice, together with the accelerating deployment of wind and solar power. These scenarios envision net global emissions (anthropogenic emissions minus anthropogenic sinks) approaching zero by the end of the century, but not necessarily enough to deliver the common 2°C goal. We compare these scenarios with 3 others: a scenario that abandons further efforts to strengthen climate policy; a scenario that incorporates the current effort of the INDC process for COP-21; and a scenario which deliberately targets 2°C but requires a policy response far stronger than the UNFCCC process is currently delivering.

In comparison to our previous study (Prinn *et al.*, 2011) that compared the scenarios developed by different groups: intergovernmental (represented by the Intergovernmental Panel on Climate Change), government (represented by the U.S. government Climate Change Science Program) and industry (represented by the Shell 2008 scenarios), here we provide not only the resulting climate variables (CO_2 and other GHG concentrations, radiative forcing, temperature) of the different emission scenarios, but also their impacts on sea level rise, oceanic acidity, water availability, air quality, and agricultural yields. This new study thus enhances our approach for integrating impacts into our modeling framework by developing modules that represent physical impacts (Reilly *et al.*, 2013).

This report provides the outputs of this study and is organized in the following way. In Section 2 we describe the scenarios and the models used. Section 3 provides the climate results, while the following 4 sections assess the resulting climate impacts. Specifically, Section 4

Table 1. Emission scenarios.

Scenario	Description
NCP2020	Copenhagen commitments through 2020 and no climate policy thereafter
Outlook	Derived from an assessment of COP-21 based on Intended Nationally Determined Contributions (INDCs) of major emitting countries
Oceans	Includes a large role for renewables and oil, and slow development of CCS
Mountains	Includes a large role for renewables after 2050, larger natural gas resources, and accelerated development of CCS
2°C	Assumes a globally uniform carbon tax starting in 2020 that leads to a global temperature stabilization of 2°C above preindustrial by 2100

discusses implications of the scenarios for sea level rise and ocean acidification, Section 5 addresses water stress, Section 6 focuses on air pollution impacts, and Section 7 looks at the changes in agricultural yields over the century. We provide concluding remarks in Section 8.

2. EMISSION SCENARIOS AND MODELING SYSTEM

In this study we focus on five emission scenarios that allow a comparison of climate change implications of the different scenarios and their impacts on sea level rise, ocean acidity, water stress, air quality, and agricultural yields. The scenarios are presented in **Table 1**.

The range of scenarios is chosen to represent quite different approaches to scenario construction. The assessment of the likely results from the COP-21 meeting (*Outlook*), plausible scenarios of the energy system development (*Oceans* and *Mountains*) and desired scenario (*2°C*) are evaluated against a "no climate policy" projection (*NCP2020*). These approaches—the likely (forecasts), the plausible (exploratory scenarios) and the desired (normative scenarios)— also comprise the three typical approaches to speaking about the future in business, government and academia.

The Shell Scenarios Team has been long recognized for its innovative use of scenario analysis to understand potential energy-economic and societal futures. Similar to our previous Shell-MIT collaboration (Prinn *et al.*, 2011), we calibrated the Shell projections for the *Oceans* and *Mountains* scenarios for the use in the MIT Integrated Global Systems Modeling (IGSM) framework (Prinn *et al.*, 2011; Prinn, 2013) that consists of the Economic Projection and Policy Analysis (EPPA) model linked to the MIT Earth System Model (MESM). The schematic of the IGSM is provided in **Figure 1**.

The MESM is a climate-chemistry model of intermediate complexity, which couples a zonally-averaged model of atmospheric dynamics and chemistry, a thermodynamic sea-ice model, a land model with an ecosystem biogeochemistry model, and a mixed layer/anomaly diffusing ocean model representing the processes of heat and carbon uptake. Climate sensitivity and the rate of oceanic uptake of heat and carbon of the MESM can be varied by changing strength of cloud feedback and value of the ocean diffusion coefficient (Sokolov, 2006). The value for median climate sensitivity (CS=2.5) is different from the previous analysis (with CS=2.9 based on Sokolov *et al.*, 2009) where Shell scenarios were used (Prinn *et al.*, 2011) due

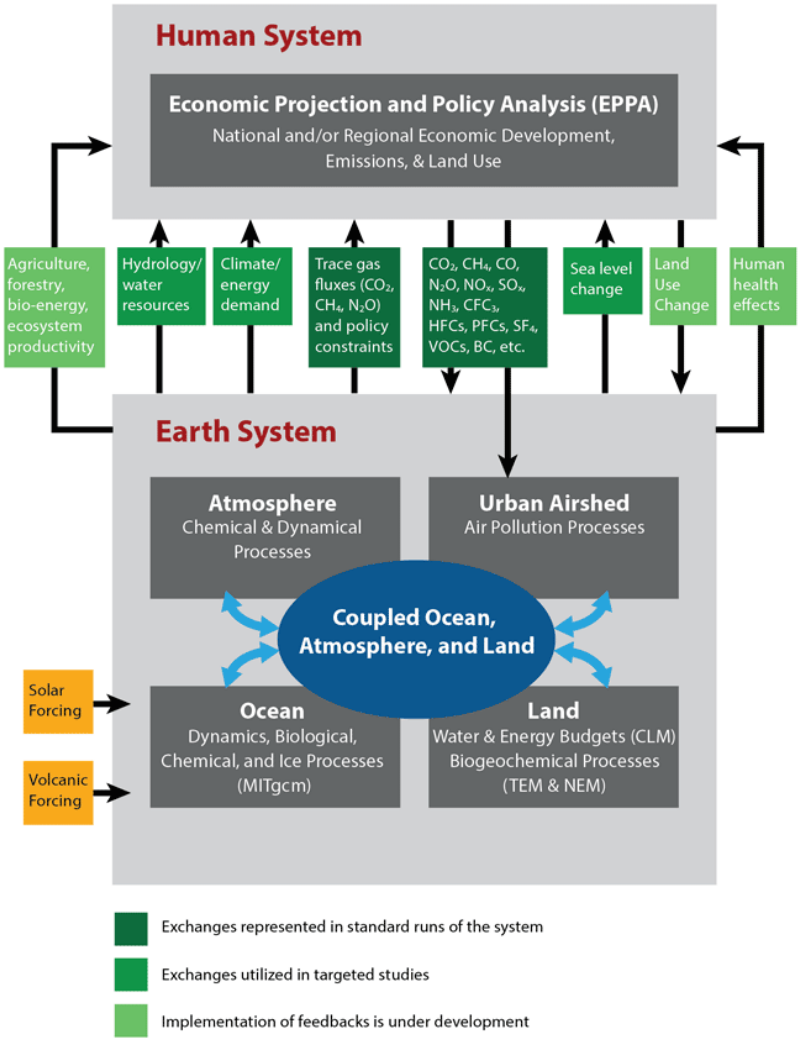

Figure 1. The MIT Integrated Global System Modeling Framework

to a different ocean model configuration and the updates in the value of ocean heat uptake (Monier *et al.*, 2013). The MESM incorporates a fully coupled chemistry model which simulates 33 species (Wang *et al.*, 1998) with 41 gas-phase and 12 heterogeneous reactions. Some chemical species, including ozone, are simulated only in the troposphere. Prescribed stratospheric ozone is used in the radiation calculations. The MESM can be run in either concentration-driven or emissions-driven mode. Values for the rate of oceanic heat uptake and strength of aerosol forcing are chosen to ensure consistency of projected historical surface warming with available observations. The rate of carbon uptake by the ocean is linked to the rate of heat uptake, based on the results of the simulations with the MIT OGCM (Dutkiewicz *et al.*, 2005; Sokolov *et al.*, 2007). The value of the CO_2 fertilization rate in the terrestrial ecosystem model (Melillo *et al.*, 2012) is chosen so that total carbon uptake in 1990–2000 was similar to observations in all simulations.

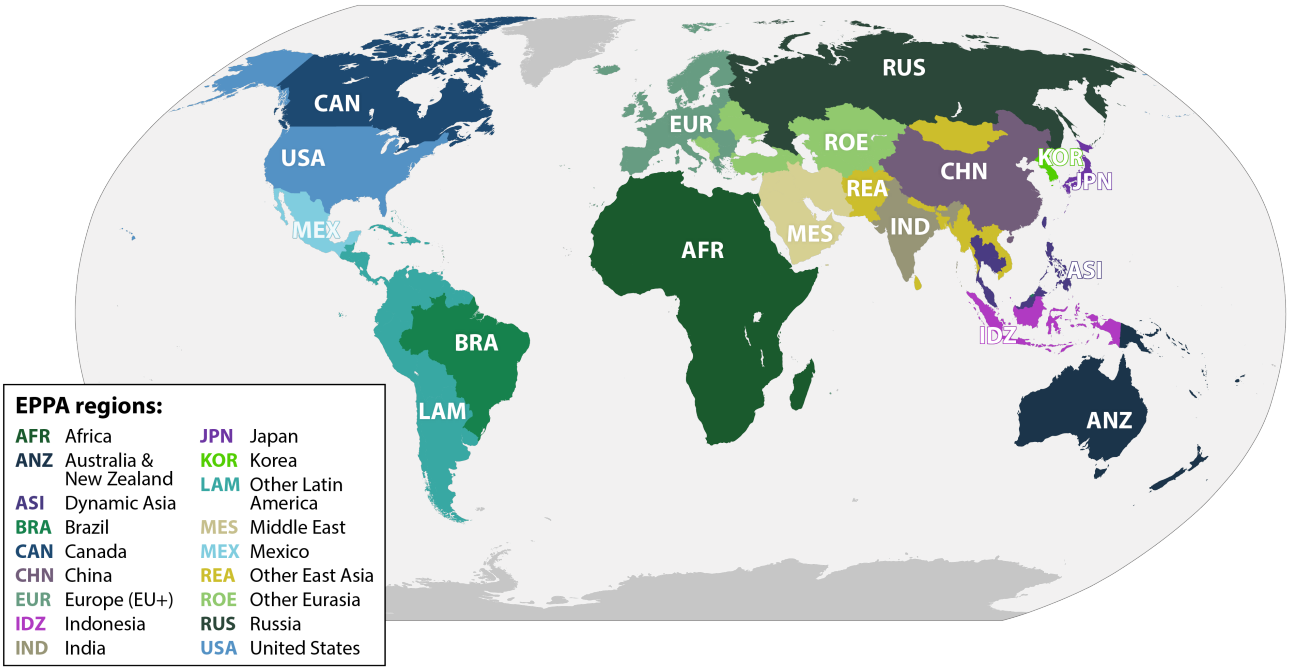

Figure 2. Regions in the EPPA model

To evaluate long-term scenarios of energy and economic development we employ the MIT Economic Projection and Policy Analysis (EPPA) model (Paltsev *et al.*, 2005; Chen *et al.*, 2015), which provides a multi-region, multi-sector dynamic representation of the global economy. The GTAP data set (Narayanan *et al.*, 2012) provides the base information on the input-output structure for regional economies, including bilateral trade flows. We aggregate the data into 18 regions and 21 sectors (sectoral details are provided in Chen *et al.*, 2015). The base year for the model is 2010, based on the calibration of the GTAP data for 2004 and 2007, and from 2010 the model solves at 5-year intervals. We also further calibrate the data for 2010–2015 based on the data from IMF and IEA (IMF, 2015; IEA, 2014). **Figure 2** represents geographical regions represented explicitly in the EPPA model.

The model includes representation of CO_2 and non-CO_2 (CH_4, N_2O, HFCs, PFCs and SF_6) greenhouse gas emissions abatement, and calculates reductions from gas-specific control measures as well as those occurring as a byproduct of actions directed at CO_2. The model also tracks major air pollutants: sulfates (SO_x), nitrogen oxides (NO_x), black carbon (BC), organic carbon (OC), carbon monoxide (CO), ammonia (NH_3), and non-methane volatile organic compounds (VOCs).

Future scenarios can be calibrated to specified energy or emission profiles or driven by economic growth (resulting from savings and investments) and by exogenously specified productivity improvement in labor, energy, and land. Demand for goods produced from each sector increases as GDP and income grow; stocks of limited resources (e.g., coal, oil and natural gas) deplete with use, driving production to higher cost grades; sectors that use renewable resources (e.g., land) compete for the available flow of services from them, generating rents. Combined with policy and other constraints, these drivers change the relative economics of

different technologies over time and across scenarios, as advanced technologies only enter the market when they become cost-competitive.

The production structure for electricity is the most detailed of all sectors, and captures technological changes that will be important to track under a GHG emission mitigation policy. The deployment of advanced technologies is endogenous to the model. Advanced technologies, such as cellulosic biofuel or wind and solar technologies, enter the market when they become cost competitive with existing technologies. Technologies are ranked according to their levelized cost of electricity, plus additional integration costs for wind and solar. When a carbon price exists, low carbon technologies are introduced. Initially, a fixed factor is required to represent costs of deployment (e.g. institutional costs, learning costs) for new technologies that—while competitive—require some time to penetrate into the market. The fixed-factor supply grows each period as a function of deployment until it becomes non-binding, allowing for large-scale deployment of the new technology. A complete description of the nesting structure of electricity generation in the EPPA model can be found in Paltsev et al (2005). The synthetic coal gas industry produces a perfect substitute for natural gas. The oil shale industry produces a perfect substitute for refined oil.

Figure 3 presents the energy-related CO_2 emissions in the scenarios considered in this study. Starting from about 30 Gigatonnes (Gt) CO_2 in 2010, emissions grow to about 70 Gt CO_2 by 2100 in the *NCP2020* scenario, about 50 Gt CO_2 in the *Outlook* scenario, but falling to about 7 Gt CO_2 in the *2°C* scenario. In the *Oceans* and *Mountains* scenarios, emissions continue to decline and approach zero after 2100.

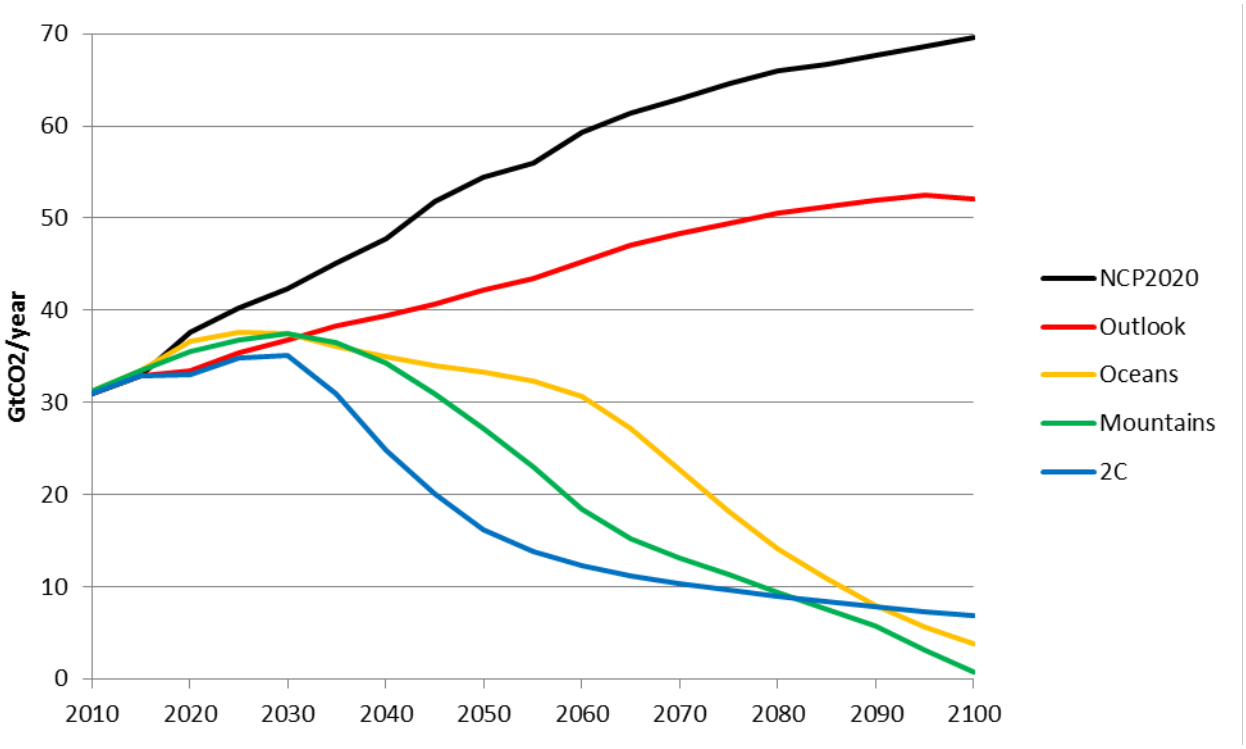

Figure 3. Energy-related CO_2 emissions

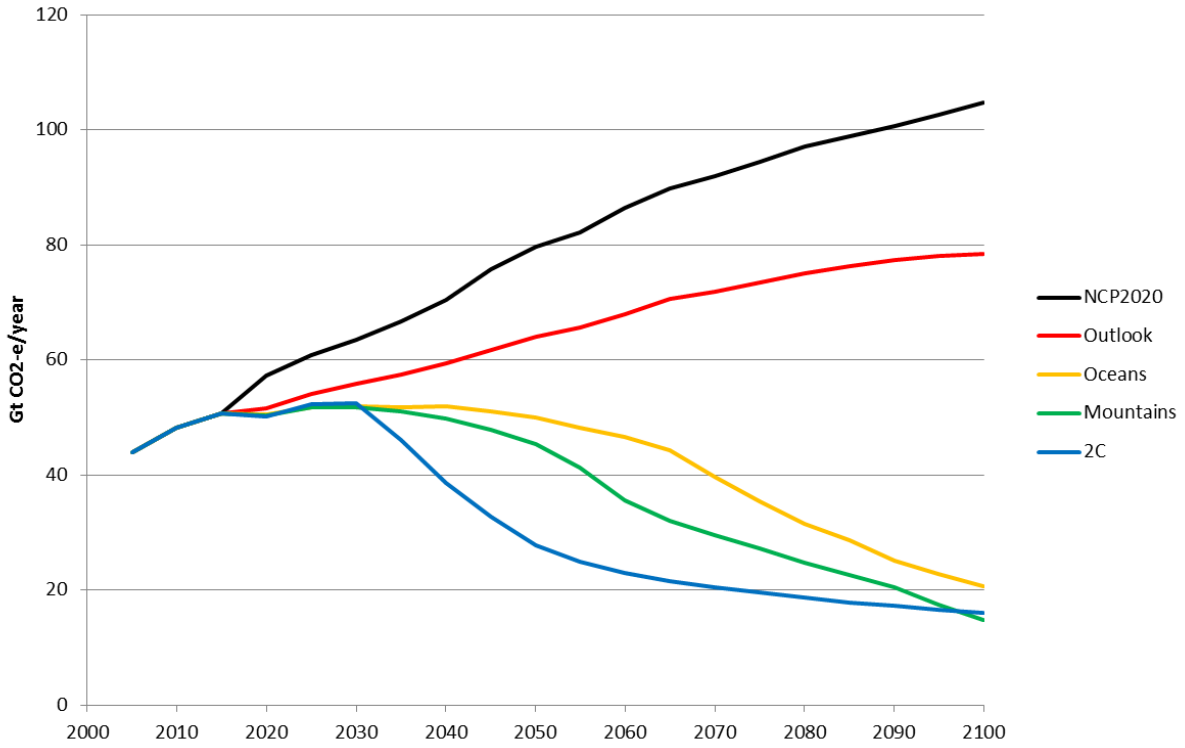

Figure 4. Total anthropogenic GHG emissions

The Shell scenarios (*Oceans* and *Mountains*) focus on the implications for the energy system, which is an important contributor to GHG emissions and the resulting global changes; however, to fully understand how human activity is affecting the planet, other important industrial and land use activities must be included. In this study we extend the Shell scenarios to capture these additional dimensions. The total anthropogenic GHG emissions are provided in **Figure 4**. They are determined not only by energy-related emissions, but by agricultural, land use, waste, and industrial energy uses and their related emissions. These activities are modelled explicitly in the MIT IGSM. Industrial non-energy CO_2 emissions are projected based on the activity of the energy-intensive cement sector. Land-use CO_2 emissions are reduced from the current levels of about 2.7 Gt CO_2 to zero by 2050, driven by implementation of deforestation-limiting policies.

3. CHANGES IN GLOBAL CONCENTRATIONS AND TEMPERATURES

The resulting CO_2 concentrations are provided in **Figure 5**. In the *NCP2020* scenario they grow from the current about 400 parts per million (ppm) in 2015 to about 805 ppm in 2100 (the average over 2091–2100 is 778 ppm). The *Outlook* scenario results in 710 ppm in 2100 (the average over 2091–2100 is 687 ppm). The *Oceans* scenario grows to about 520 ppm in 2100 (the average over 2091–2100 is 524 ppm), while the *Mountains* scenario ends up at about 500 ppm in 2100 (the average over 2091–2100 is 499 ppm). The *2°C* scenario results in about 480 ppm by 2100 (the average over 2091–2100 is 478 ppm).

Figure 6 provides the results for total GHG concentrations in terms of the CO_2 equivalents. In the *NCP2020* scenario they grow from the current 450 ppm in 2015 to about 1200 ppm in 2100. The

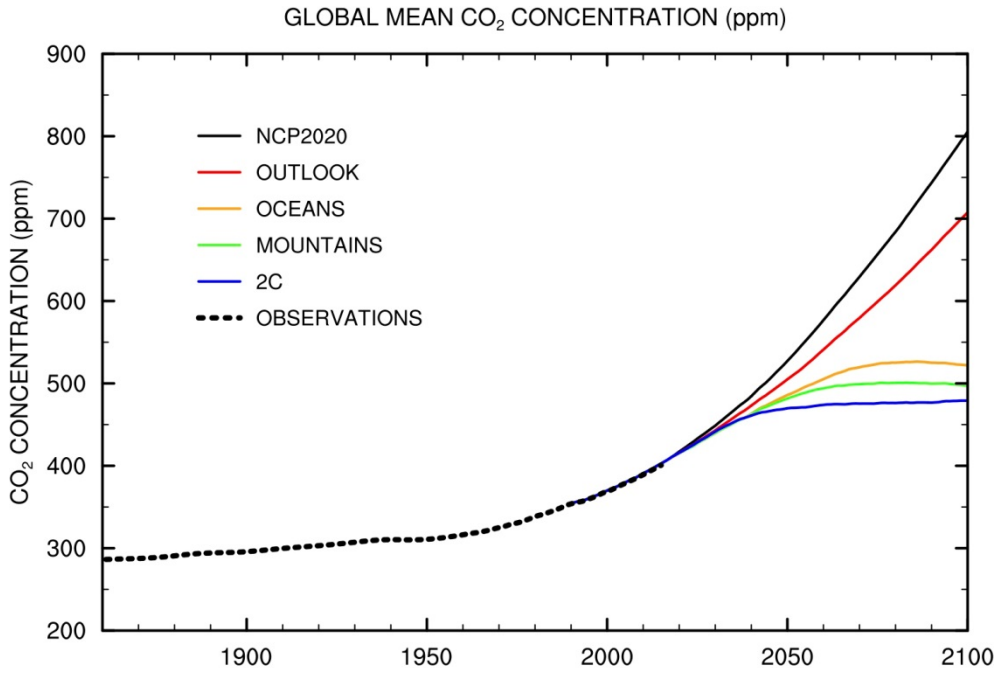

Figure 5. CO_2 concentrations

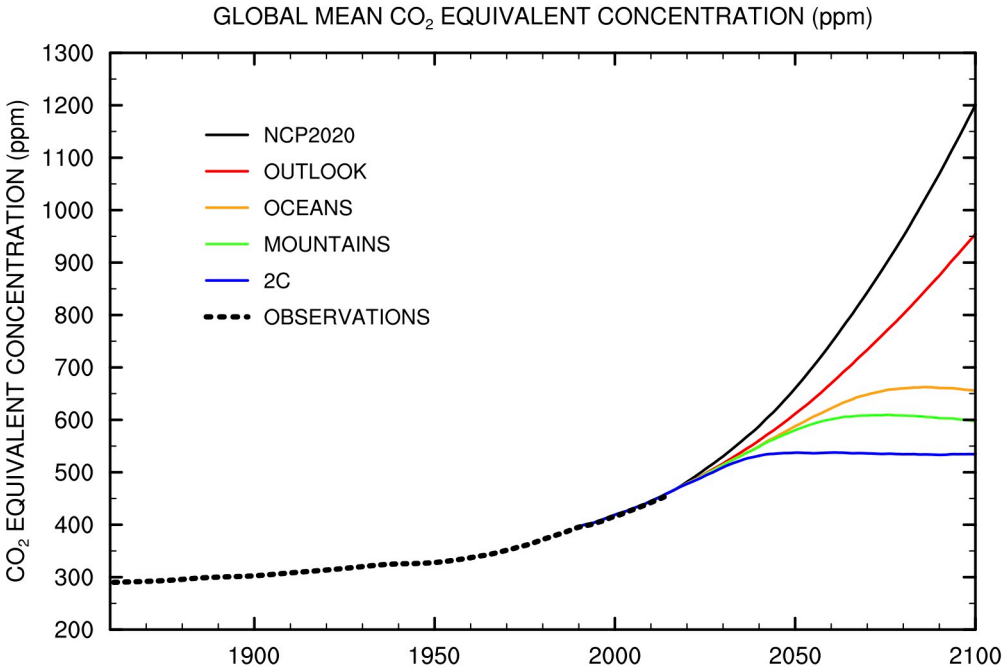

Figure 6. Equivalent CO_2 GHG concentrations

Outlook scenario results in about 910 ppm in 2100. The *Oceans* scenario grows to about 660 ppm in 2100, while the *Mountains* scenario results in about 600 ppm in 2100. The *2°C* scenario results in about 540 ppm by 2100. The corresponding averages over 2091–2100 are 1141 ppm for *NCP2020*, 919 ppm for *Outlook*, 659 ppm for *Oceans*, 601 ppm for *Mountains*, and 534 ppm for the *2°C*.

The results for total radiative forcing are provided in **Figure 7**. Radiative forcing depends on the changes since preindustrial in levels of GHGs, sulfate and black carbon aerosols, and ozone. It is a measure of the difference between the energy (sunlight) absorbed by the Earth and the energy radiated back to space. The current (year 2015) value for radiative forcing is about 2.5 watts per square meter of the Earth surface (W/m^2). By 2100, in the *NCP2020* scenario it grows to 7.8 W/m^2. The corresponding values are 6.6 W/m^2 in the *Outlook* scenario, 4.8 W/m^2 in the *Oceans* scenario, 4.2 W/m^2 in the *Mountains* scenario, and 3.5 W/m^2 in the *2°C* scenario.

The results for the annual mean surface air temperature relative to pre-industrial levels are provided in **Figure 8**. The current (year 2015) anomaly is about 1°C relative to pre-industrial levels. In terms of an average temperature increase in 2091–2110 relative to pre-industrial, the *NCP2020* scenario grows by 4.25°C (the average over 2091–2100 is 4°C), the *Outlook* scenario by 3.6°C (the average over 2091–2100 is 3.4°C), the *Oceans* scenario by 2.7°C (the average over 2091–2100 is 2.7°C), the *Mountains* scenario by about 2.44°C (the average over 2091–2100 is 2.5°C), and the *2°C* scenario by 2°C. Figure 8 shows that the world is on a path to a pre-determined temperature increase by 2040–2050 regardless of the emissions scenario. These changes are expected to occur because even the most aggressive actions to reduce emissions would not immediately eliminate the impacts of past anthropogenic emissions on climate due to the substantial inertia in Earth processes, especially oceanic heat uptake.

The IGSM pattern-scaling technique (Schlosser *et al.*, 2013) was employed and utilized patterns of precipitation and surface-air-temperature, estimated from the Coupled Model Intercomparison Project Phase 3 (CMIP3) climate models. We focus our attention on two particular pattern changes as estimated from climate models developed by the National Center for Atmospheric Research (herein, referred to as "pattern N") as well as that of the Model for Interdisciplinary Research on Climate (herein, referred to as "pattern M"). Regional temperature changes are provided in **Figure 9**. Note that the regional changes are shown relative to the 1991–2010 mean due to lack of regional observations at the earlier date. The polar regions are affected more than the tropical regions.

The results for global precipitation changes are provided in **Figure 10**. The historic values for the global mean precipitation averaged over 1861–1880 period is 2.66 mm/day and averaged over the 1991–2010 period is 2.7 mm/day. In the *NCP2020* scenario the mean 2091–2100 global precipitation grows by 10.3% relative to pre-industrial. The *Outlook* scenario results in the corresponding 8.7% increase. The *Oceans* scenario reduces the precipitation anomaly to a 7.4% increase, and the *Mountains* scenario to a 6.6% increase. The *2°C* scenario results in only a 5.5% increase. Regional precipitation impacts are provided in **Figure 11**. Note that the regional impacts are shown relative to the 1991–2010 mean due to lack of regional observations at the earlier date. There is sometimes a variation in regional precipitation between the two different scaling patterns (M, N), for example, over the North Atlantic and Indian Oceans. At the same time, the two different patterns agree for changes in some other areas like a decrease in precipitation in Central America and an increase in precipitation in Central Africa and parts of East Asia.

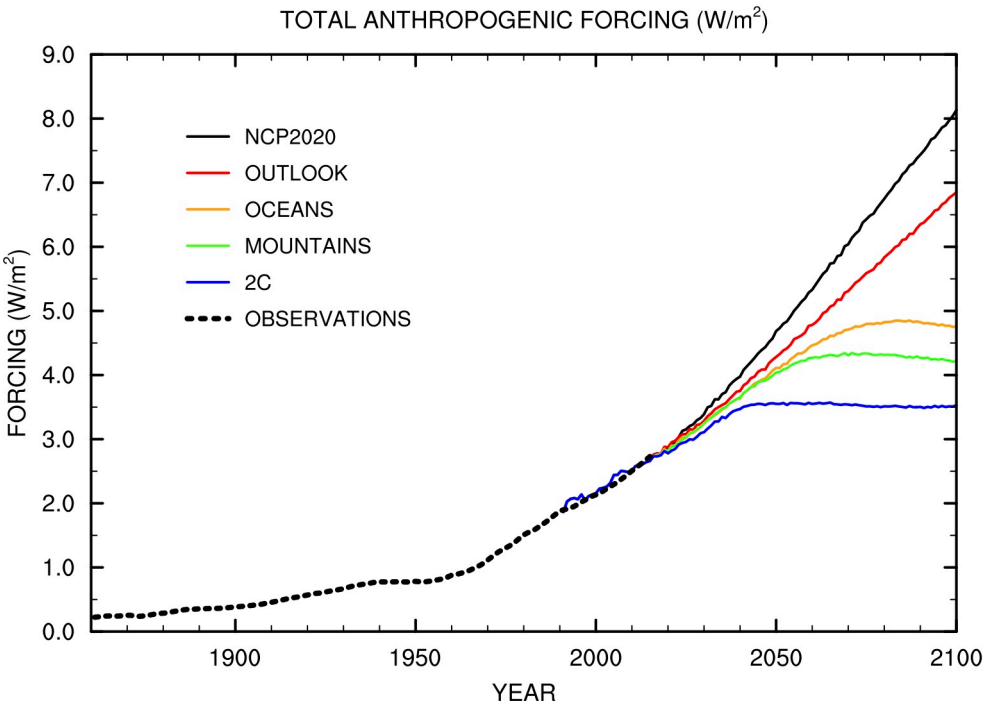

Figure 7. Total Radiative Forcing

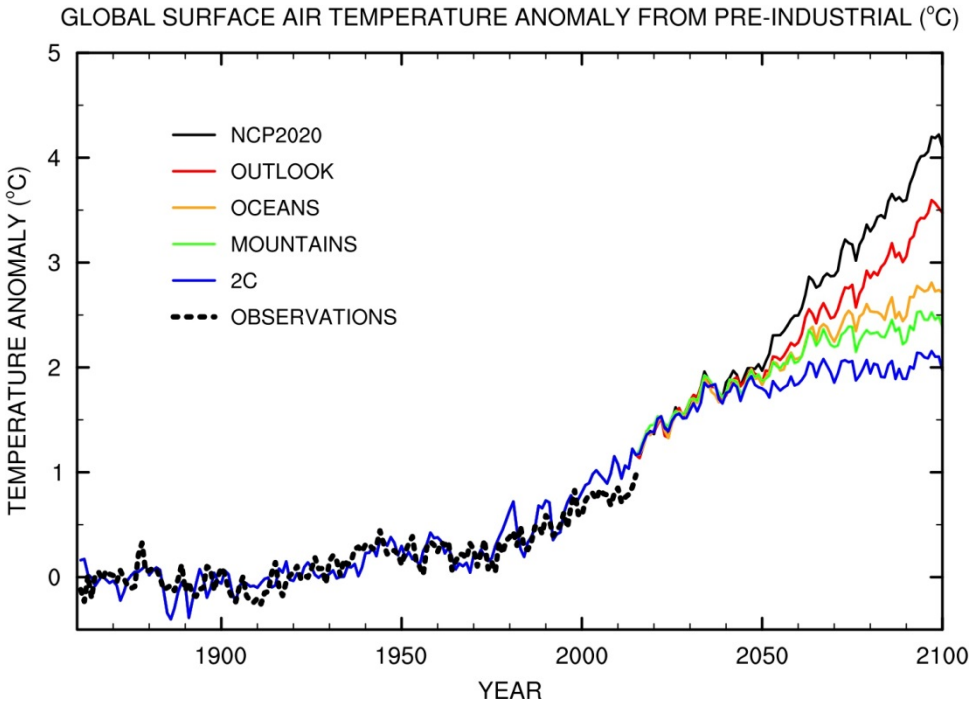

Figure 8. Global temperature changes relative to preindustrial levels.

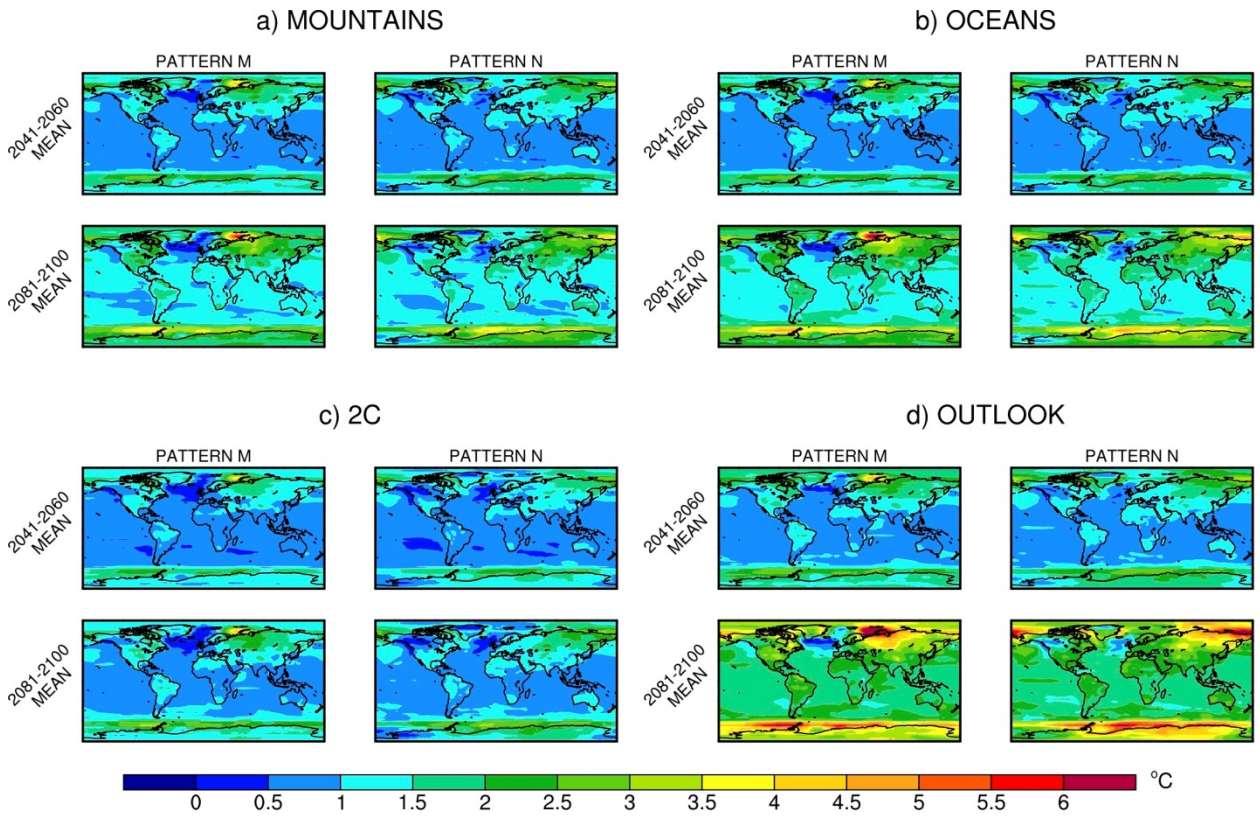

Figure 9. Regional temperature changes relative to the 1991–2010 mean.

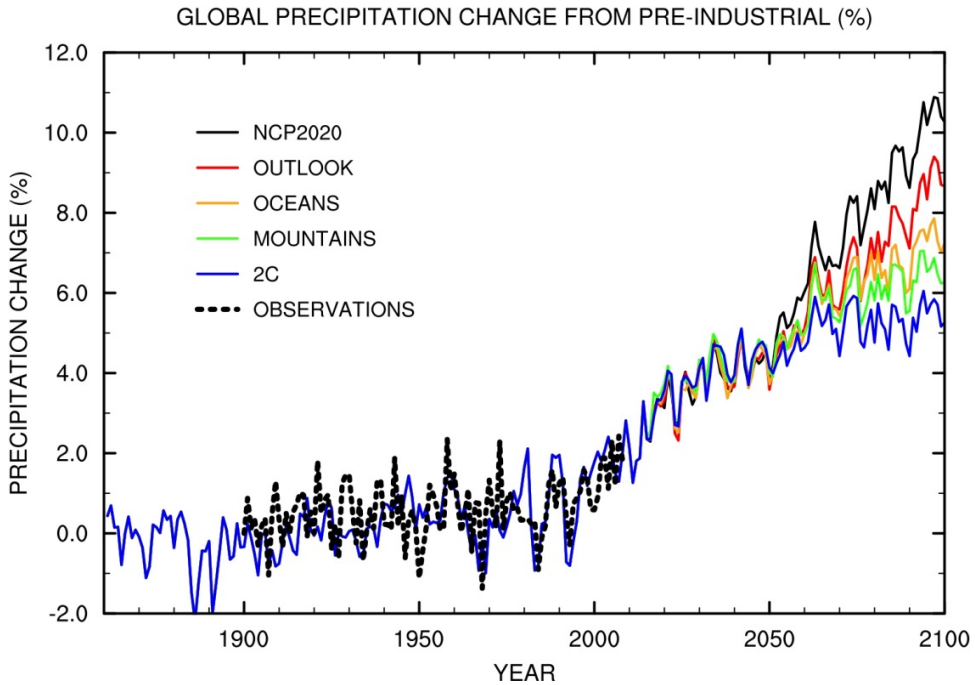

Figure 10. Global precipitation change (%) relative to pre-industrial

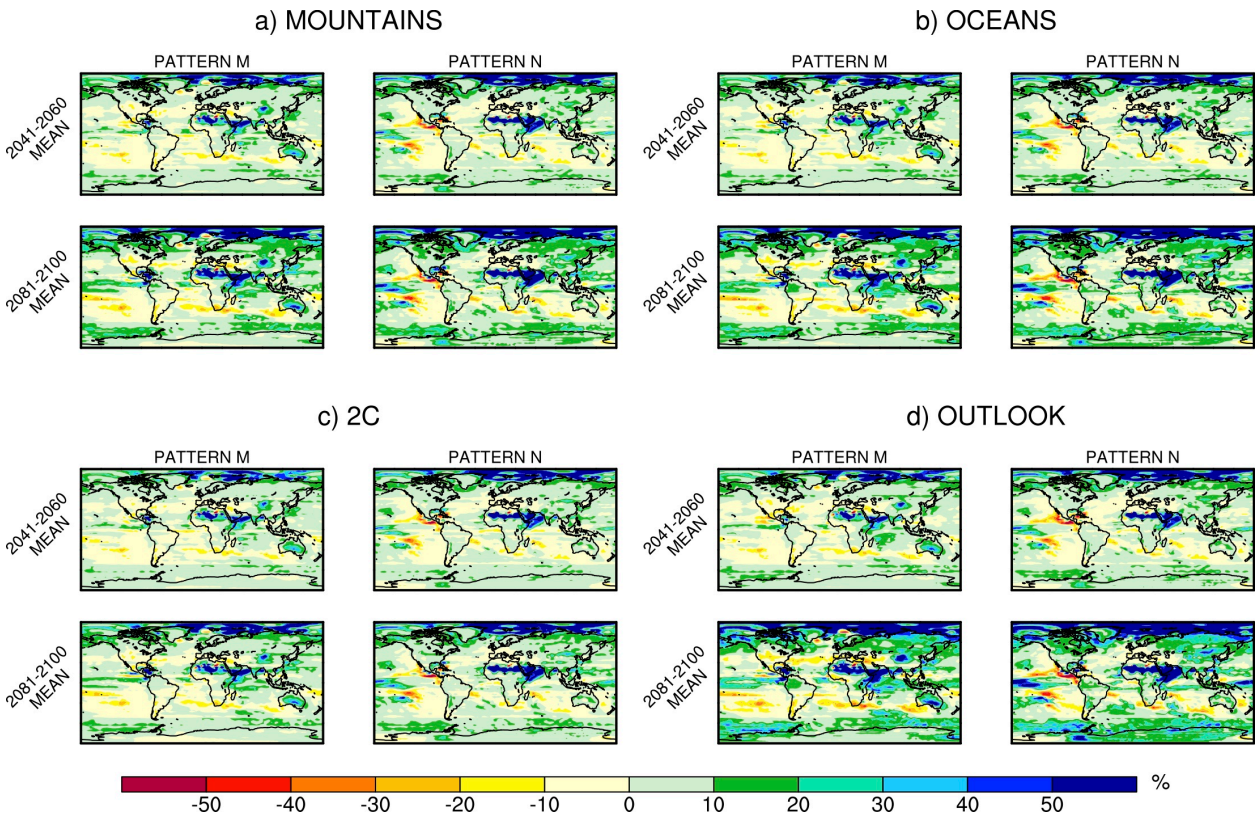

Figure 11. Regional precipitation change (%) relative to 1991–2010 mean.

4. CLIMATE IMPACTS ON OCEAN ACIDITY AND SEA LEVEL RISE

Oceanic acidification refers to chemical changes in the ocean as a result of the uptake of carbon dioxide from the atmosphere. **Figure 12** shows the already ongoing increase in acidity (measured by a decrease in the logarithmic scale of pH). A decrease of 1 in this scale corresponds to a factor of 10 increase in acidity. The *NCP2020* and *Outlook* scenarios show a decrease in oceanic pH from the current about 8 to about 7.75–7.8. The levels of 7.7–7.8 would significantly impact all calcareous phytoplankton that are the base of the ocean food chain (Prinn *et al.*, 2011). The *Oceans*, *Mountains*, and *2°C* scenarios result in a much smaller impact. The *Oceans* and *Mountains* scenarios are at about 7.92–7.94 by 2100, while the *2°C* stabilization scenario achieves about 7.95 by 2100. The Shell scenarios (*Oceans* and *Mountains*) and the *2°C* scenario cap the damage, while the *NCP2020* and *Outlook* scenarios are heading toward further damages in the 22nd century.

Figure 13 provides the spatial resolution for the oceanic pH results. The blue colors represent the "dangerous" territory of pH of 7.7–7.8, which is achieved by 2100 in the *Outlook* scenario. The *Oceans* and *Mountains* scenarios reduce the impact significantly (yellow and green lines in the figure). They are close to the *2°C* scenario impacts (blue line, pH of 7.95).

The results for sea level rise (in meters) due to thermal expansion and melting of mountain glaciers are provided in **Figure 14**. These projections do not include the possible substantial additions from melting Greenland and Antarctic ice sheets. At present, ice sheet sub-models are not

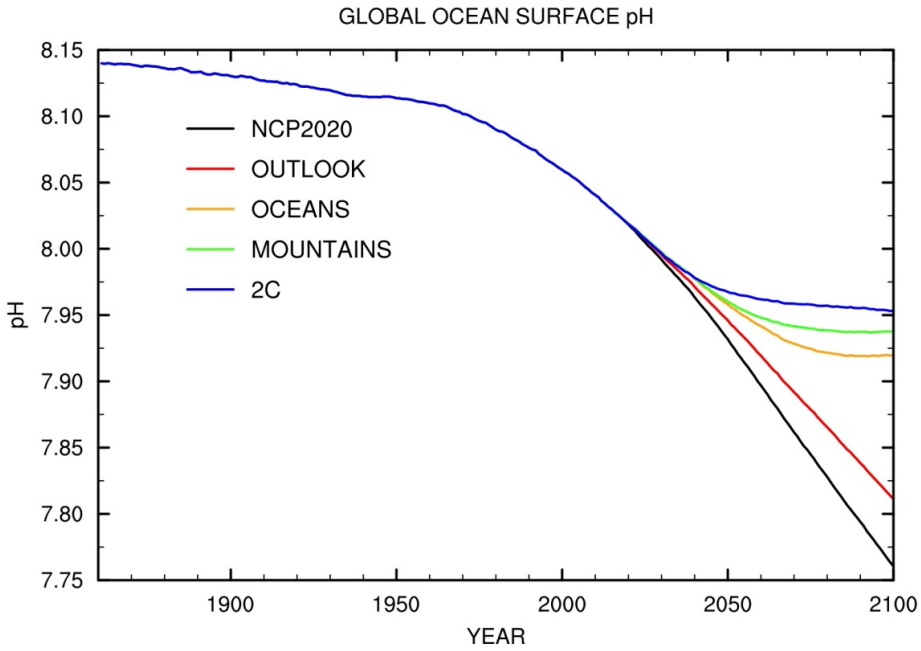

Figure 12. Oceanic pH ($-\log_{10}[H^+]$)

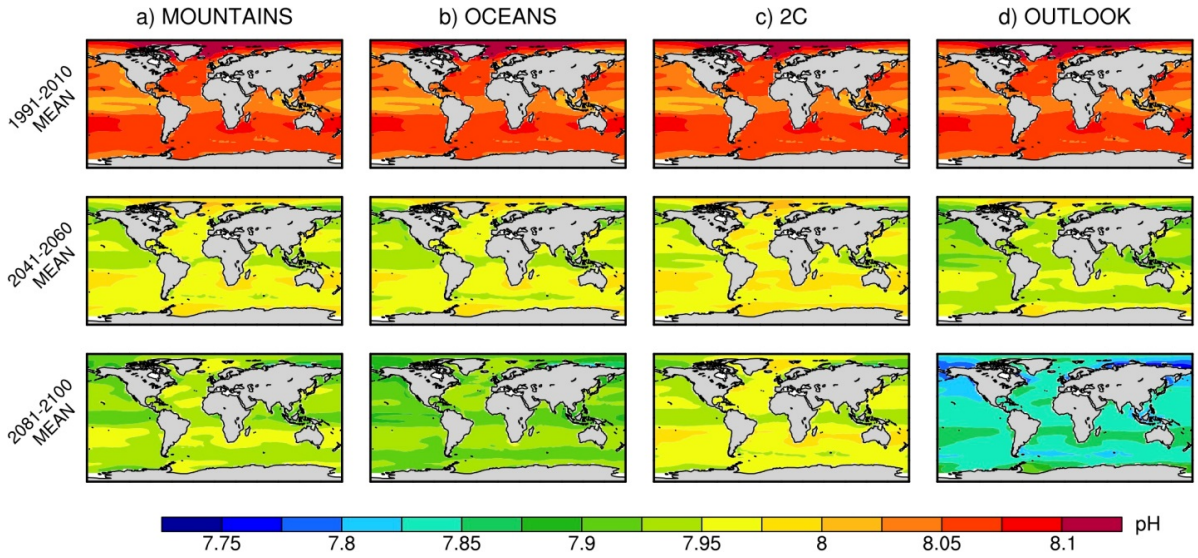

Figure 13. Spatial changes in oceanic pH

included in IGSM because of inadequate understanding of the processes that explain the current melting. The majority of the masses of these ice sheets should remain frozen through the course of this century; however recent evidence suggests that the anticipated portion that will melt would contribute non-negligibly to sea level rise by 2100. However, uncertainties among the most recent assessments from the IPCC 5th Assessment Report (Bindoff *et al.*, 2013) as well as model-based estimates (e.g. Fetweiss *et al.*, 2013 and Yang *et al.*, 2014) of the Greenland and Antarctic ice sheet contribution to sea-level rise through 2100 is notable. Excluding the impact of a collapse in the marine-based sectors of the West Antarctic ice sheet, total ice-sheet contributions to sea-level rise

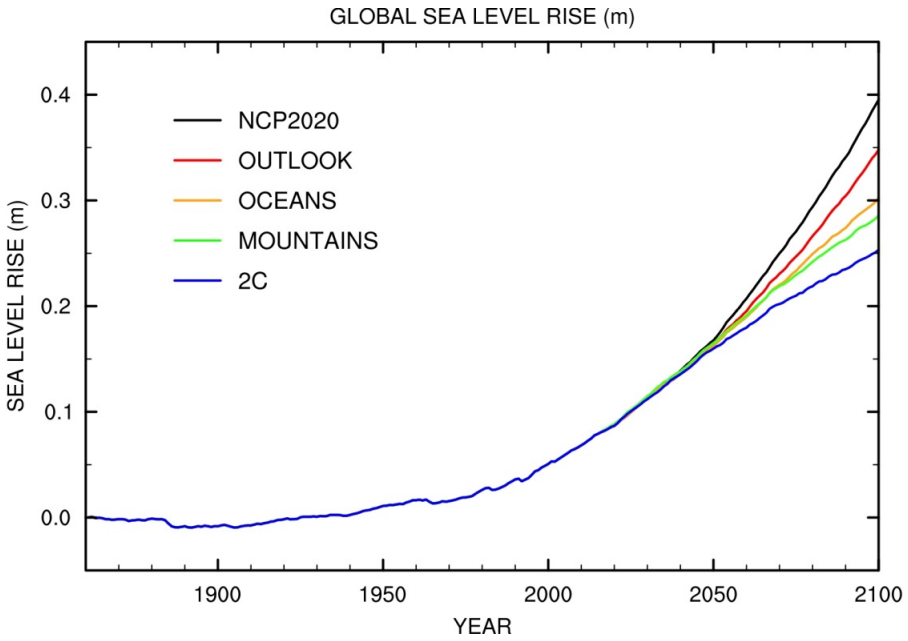

Figure 14. Sea level rise due to thermal expansion and melting of mountain glaciers

by 2100 can range from 0 to up to 0.40 meters for the Representative Concentration Pathway (RCP) 4.5 case (aligned with the *Mountains* and *Oceans* scenarios' radiative forcing), and from 0 up to 0.9 meters for the RCP 8.5 case (aligned with the *NCP2020* scenario). Should the west Antarctic ice sheet collapse, it is estimated this would contribute an additional several tenths of a meter by 2100 (IPCC, 2013). Further considerations including uncertainties in model assumptions of basal sliding (over Greenland) could remove any likelihood of no contribution to sea level rise in this century. Nevertheless, given the disparity in these model-based estimates, one can also extrapolate as a prognostic proxy the recent trends in the Greenland and Antarctica mass balances as observed by satellite-retrieval methods (and corroborated by in situ measurements). Estimates of ice-mass loss from The Gravity Recovery and Climate Experiment (GRACE) retrievals have been documented (e.g. Velicogna *et al.*, 2014). Since 2003, mass loss rates for Greenland and Antarctica are approximately 268 and 67 Gt/year, respectively. These values translate into eustatic sea-level changes of 0.74 and 0.19 mm/year, respectively. If we were to extrapolate these loss rates through the rest of the 21st century, we can expect a combined sea-level rise from these ice sheets of approximately 33 mm by 2050 and 79 mm by 2100. For this calculation, we do not consider the ice-loss rate acceleration as estimated by GRACE, due to shortness of the data record (which a number of investigators note). Indications are that the error in the GRACE mass loss rates estimates are on the order of ±20%. Therefore, we can also place approximate bounds to these extrapolated cumulative sea-level rise estimates to be 33±6 mm rise by 2050 and 79 ±14 mm rise by 2100. While this observation-based projection falls within the broad range of the aforementioned model-based estimates, it further underscores that if the recent observed retreats in the large ice sheets are to continue through the course of this century, they would contribute a notable addition to the sea level rise estimates shown in Figure 14 (~20% of all scenarios at 2050 and ~17.5% of the *NCP2020* scenario as well as up to 28% of the *2°C* scenario by 2100).

5. CLIMATE IMPACTS ON WATER STRESS

We have assessed the trends in water stress using the Water Resource System (Strzepek *et al.*, 2013) forced by the global simulations of climate change (Section 3) as well as the socio-economic drivers of the IGSM. Similar to previous work (e.g., Schlosser *et al.*, 2014; and Blanc *et al.*, 2014) we assess changes in water stress for the globe at 282 Assessment Sub-Regions (ASRs), which are geographic regions delineated by large river basin and country boundaries. At each ASR, we calculate a Water Stress Index (WSI) as the ratio of total water withdrawals to the total surface water supply (sum of the basin's runoff and inflow from upstream basins). The changes in WSI are assessed with respect to the WRS forced by observed historical climate conditions (**Figure 15**). Values of WSI greater than 0.3 are regarded as experiencing "moderately" stressed conditions, and values greater than 0.6 characterized as "heavily" stressed. WSI values greater than 1 indicate ASRs with severe (deficit) water stress conditions.

The simulations using WRS were performed for all five scenarios in Table 1. As mentioned in Section 3, for each of these scenarios the IGSM pattern-scaling technique was employed. Two patterns ("Pattern N" and "Pattern M") are used to assess the degree to which the range in climate model simulations of regional climate changes contribute to the overall uncertainty in our water stress assessments and the effectiveness of mitigation pathways.

Globally speaking, we find that aspects associated with the changes in WSI out to 2050–2060 are quite similar to the results of Schlosser *et al.* (2014). The largest *relative* increases in WSI are

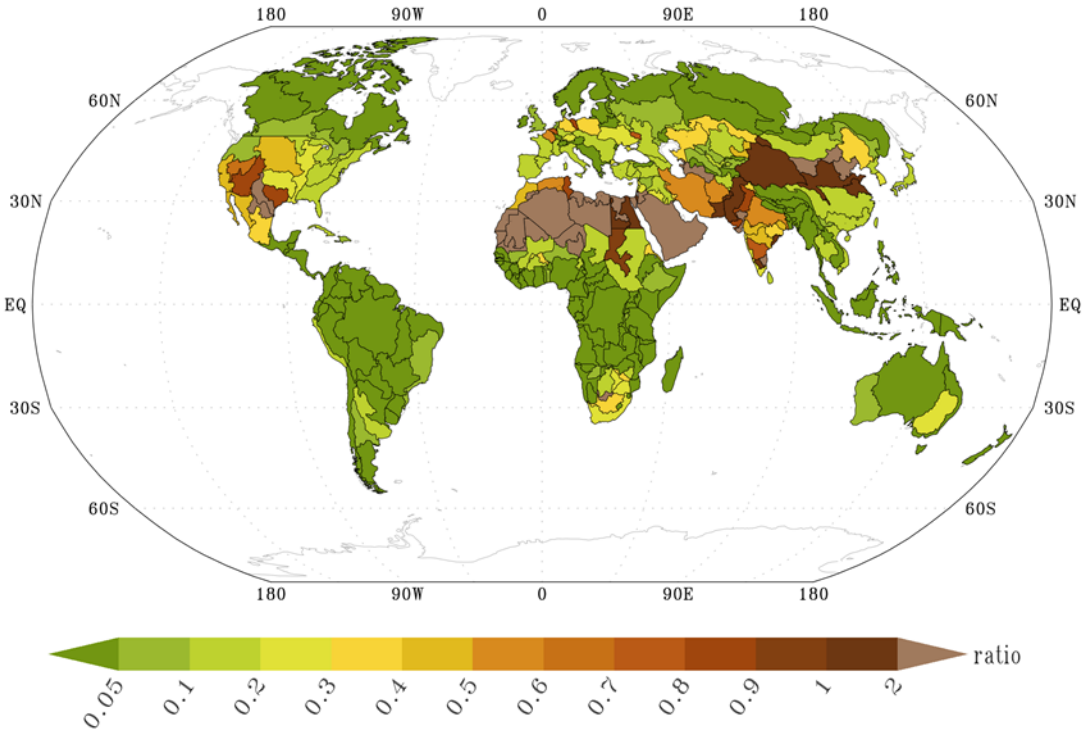

Figure 15. Water Stress Index (WSI, unitless) averaged for the years 2001–2020 from the Water Resource System simulation

found in Africa (**Figure 16**, all panels), and are primarily the result of large increases in the non-agricultural water-demand sectors (driven by increases in population and economic output). The effect of the mitigation policies is notable (bottom panel, Figure 16), yet none of the policies considered in this study are able to eradicate the widespread increases in WSI. This further underscores the finding of Schlosser *et al.* (2014) that adaptive measures will be required, worldwide, to meet surface-water shortfalls—even under the most aggressive and/or intermediate climate mitigation scenarios.

The results also highlight the importance of the uncertainty in regional climate patterns. The most notable differences in the sign and/or strength in water-stress change, as a result of the choice of climate pattern, are seen for ASRs located in developed nations or large emerging economies. Comparing the top and middle panels of Figure 16 (where differences are only a result of the climate-pattern selection), we find the largest differences over North America as well as for basins in Eastern Africa, Southern and Eastern Asia, as well as Europe. These changes are comparable to those seen, correspondingly, between the middle and bottom panels of Figure 16, which are a result solely of the choice between the *2°C* scenario and the *NCP2020* scenario.

An increase in precipitation in some parts of the globe (e.g., Northeastern Africa and parts of East Asia, as shown in Figure 11) helps to ameliorate the water situation even with the increased water demand, but in many locations the total water withdrawals increase more than the total water supply, which results in the increases in WSI. The most striking aspect of the *2°C* scenario results is the large (relative) increases in WSI that remain over most of Africa. As noted, this is a result of socio-economic growth drivers of water sector demands, and this growth is largely insensitive to the choice of climate scenario—even the most aggressive—over the coming decades (up to the middle of the century). Nevertheless, climate mitigation does seem to hold promise at buffering (and even reversing) the increased water stress from climate change over North America, Eastern and Southern-most Africa, Eastern and Southern Asia, and Australia.

The intermediate policies of the *Mountains* and *Oceans* scenarios result in some encouraging effects (**Figure 17**) to alleviate large-scale water stress. The reduction (or reversal) of WSI increases obtained from the *2°C* scenario are found—to a lesser degree—across basins in North America, Eastern Africa, Eastern and Southern Asia, and Australia.

The less notable effect of these intermediate policies is on the relative changes in irrigiation demand, with the majority of the basins across the globe resulting in marginally reduced irrigation demand increases under these scenarios (comparing left and right panels of **Figure 18**). Impacts to relative runoff change are found to be more extensive than those seen for irrigation demand (**Figure 19** shows runoff results for 2060). Basins with the strongest runoff response to climate scenarios are found in Eastern Africa as well as over North America, Asia, and the northern basins of South America.

Additional aspects of these sensitivies can also be seen when viewing the WSI time series for a particular ASR. For example, **Figure 20** shows the WSI trends of the Ganges River (India) ASR, shown as a percentage change from the mean of all simulations that we have conducted—and thus indicates the marginal impact of a scenario and its climate pattern on WSI. One of the

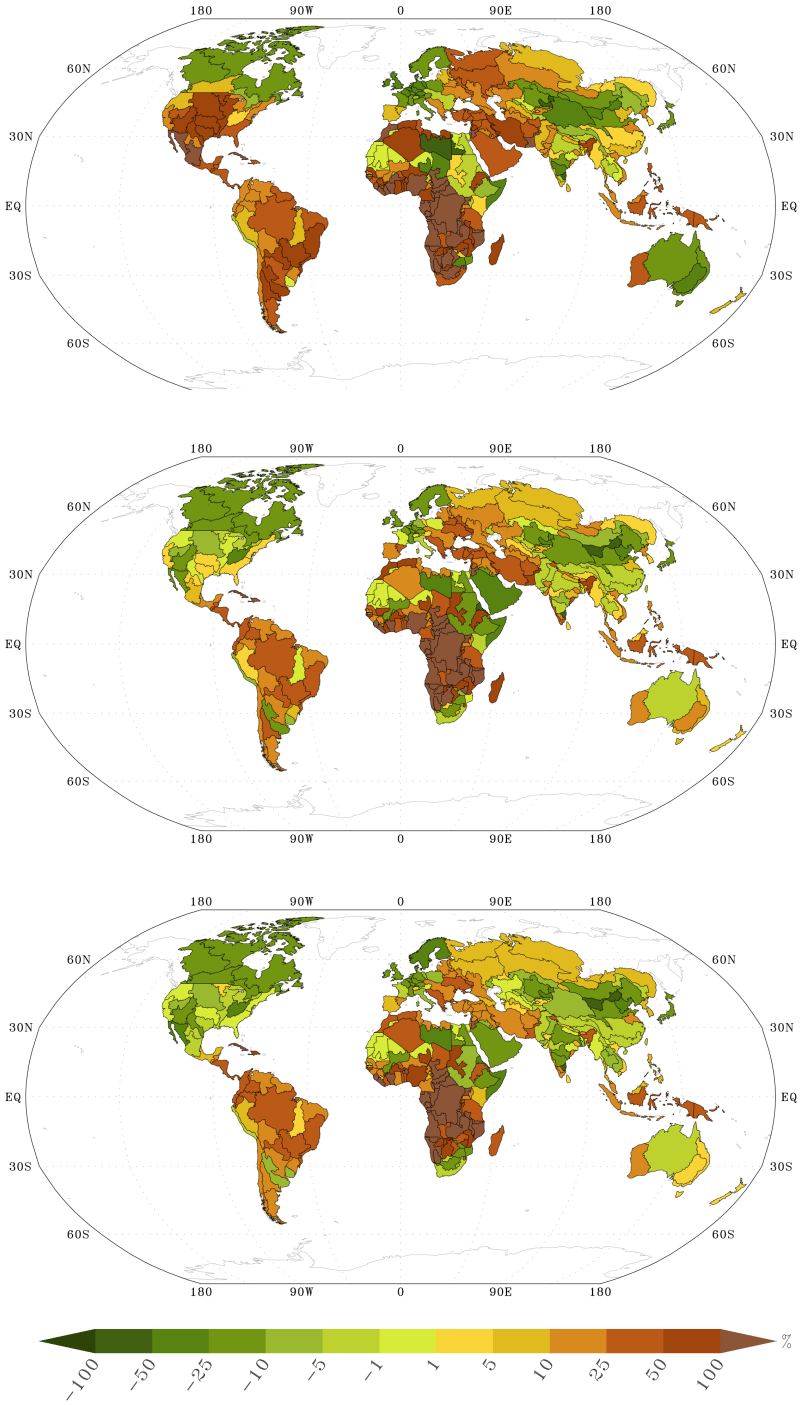

Figure 16. Changes in WSI (%), a 20-year averaged result whose calculation is centered at 2060, are shown as a percentage to the baseline value of Figure 15. Results are shown for a selection of the simulations performed with the IGSM-WRS. The top panel shows the result for the *NCP2020* scenario with "Pattern M" of climate variables. The middle panel shows the *NCP2020* scenario with "Pattern N" of climate change, and the bottom panel shows the *2°C* scenario with "Pattern N" of climate change.

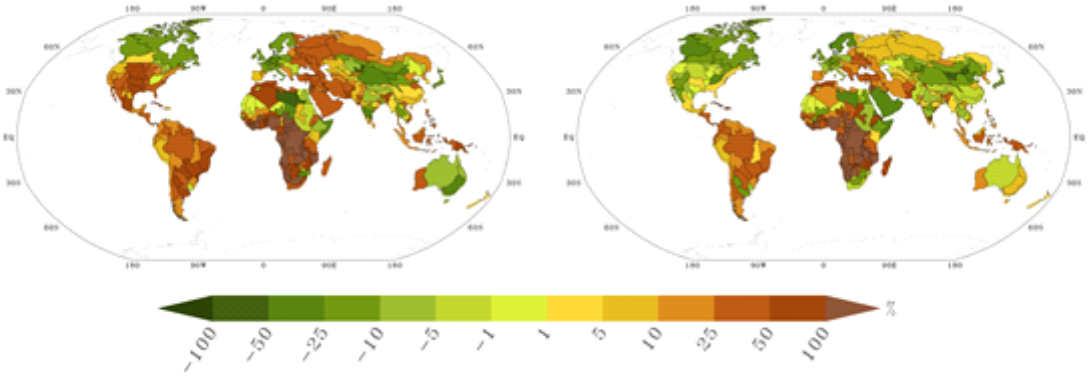

Figure 17. Relative changes in WSI (%), a 20-year averaged result whose calculation is centered at 2060, are shown as a percentage to the baseline value of Figure 15. The results are shown for selected simulations with the IGSM-WRS. The left panel shows the result for the *Mountains* scenario with "Pattern M" of climate change. The right panel shows the *Oceans* scenario with "Pattern N" of climate change.

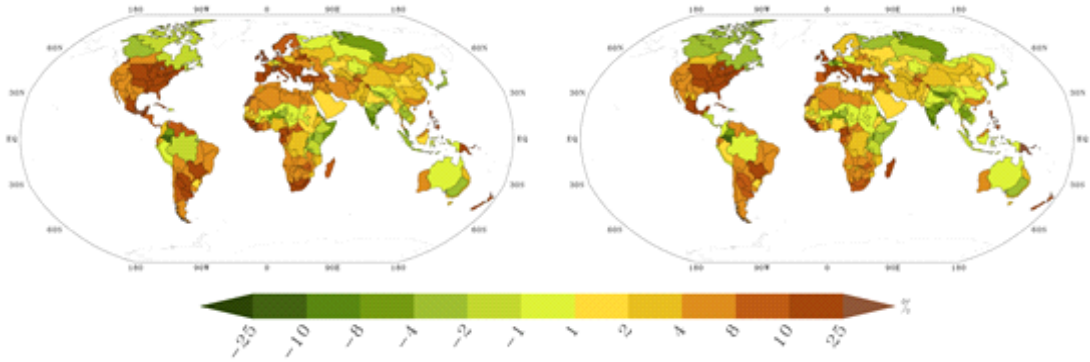

Figure 18. Relative changes in irrigation demand (%), a 20-year averaged result whose calculation is centered at 2060, are shown as a percentage to the 2001–2020 avearge. The results are shown for selected simulations with the IGSM-WRS. The left panel shows the result for the *NCP2020* scenario with "Pattern M" of climate change. The right panel shows the *Oceans* scenario with "Pattern M" of climate change.

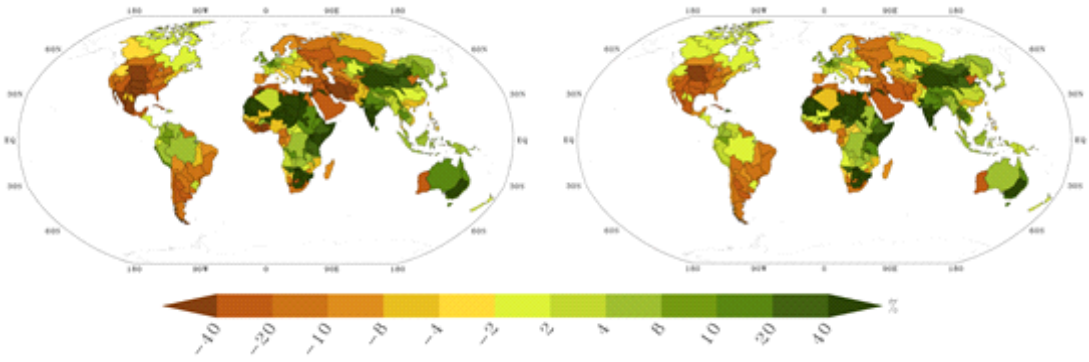

Figure 19. Relative changes in runoff (%), a 20-year averaged result whose calculation is centered at 2060, are shown as a percentage to the 2001–2020 avearge. The results are shown for selected simulations with the IGSM-WRS. The left panel shows the result for the *NCP2020* scenario with "Pattern M" of climate change. The right panel shows the *Mountains* scenario with "Pattern M" of climate change.

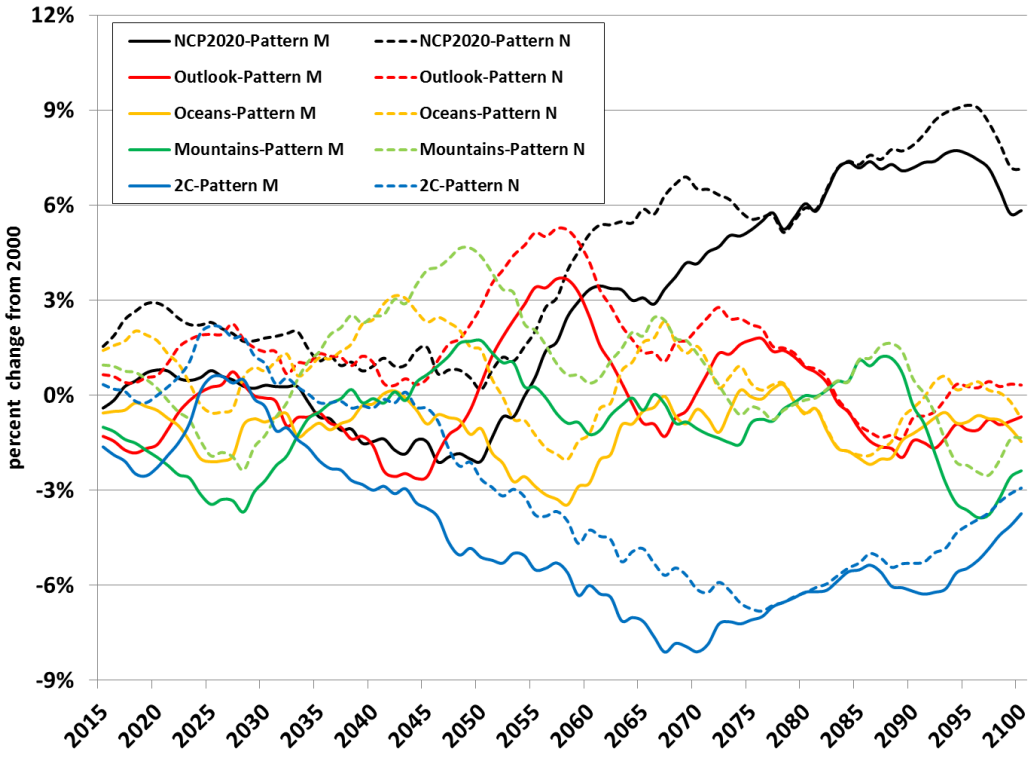

Figure 20. Time series (with a five-year running mean) of the relative change in WSI (%) for the Ganges River Basin driven by the various scenarios of future socio-economic and climate change from the Water Resource System of the IGSM. The changes in WSI for each scenario (denoted by line color) as well as climate pattern (dashed (N) or solid (M) line) are relative to the mean of all the simulations. Therefore, the values indicate the marginal effect of any scenario on WSI relative to the central/mean tendency of all the simulations.

more prominent features is the clustering of all the timeseries irrespective of the choice of the climate-change pattern (solid versus dashed lines), which persists through the 2040s. During the time period, the effect of any particular scenario is weak and difficult to discern.

We emphasize here that the choice of the two climate patterns (M,N) does not necessarily represent the total range of plausible climate outcomes. A more comprehensive sampling of climate patterns is warranted in order to determine the full range of outcomes as well as assess the likelihood of any particular WSI trend tendency (i.e., increase, decrease, or no change). Nevertheless, it is during the latter half of the 21st century where the impact of scenarios on the WSI trends emerges. In both of the climate-pattern choices, the most effective mitigation scenario is the *2°C* scenario, which by 2100, is the only policy that results in a prolonged decrease in WSI for both climate patterns. Conversely, by 2100 the *NCP2020* scenario shows the largest increase in WSI, and in addition, both of the climate patterns for this scenario are among the largest increases in WSI. The *Outlook* scenario shares a similar characterization that by 2100 both of its climate pattern results produce little change in WSI. An encouraging impact of both the *Mountains* and *Oceans* scenarios is the fact that by 2100, their climate pattern results converge to the results of no change in WSI. As noted previously, a more comprehensive sampling of climate-pattern outcomes would allow for a more quantitative assessment as the likelihood that these scenarios could provide a preventative measure of any change in water stress for the Ganges.

Globally speaking—the water-stress impact of these climate scenarios indicate that by the latter half of the 21st century, at least 1 billion to as many as 2 billion additional people will experience at least moderately stressed water conditions worldwide (**Figure 21**). However, the impact of more aggressive climate scenarios could play a notable role in mitigating these numbers. Not surprisingly, the more aggressive *2°C* mitigation scenario provides the strongest preventative effect in this regard. However, the beneficial impact of the *Oceans* scenario is also clearly seen and is quite comparable to the benefits of the *2°C* policy target. For the *Mountains* scenario, while one of the pattern outcomes indicates a strong mitigating effect on water-stressed populations, it also exhibits the strongest sensitivity to the choice of the climate pattern outcome. As previously emphasized, the lack of a full sampling of all possible climate-change patterns precludes any generalization to be made in this regard. Nevertheless, the mitigating impact of these intermediate scenarios on future water-stressed populations is substantial.

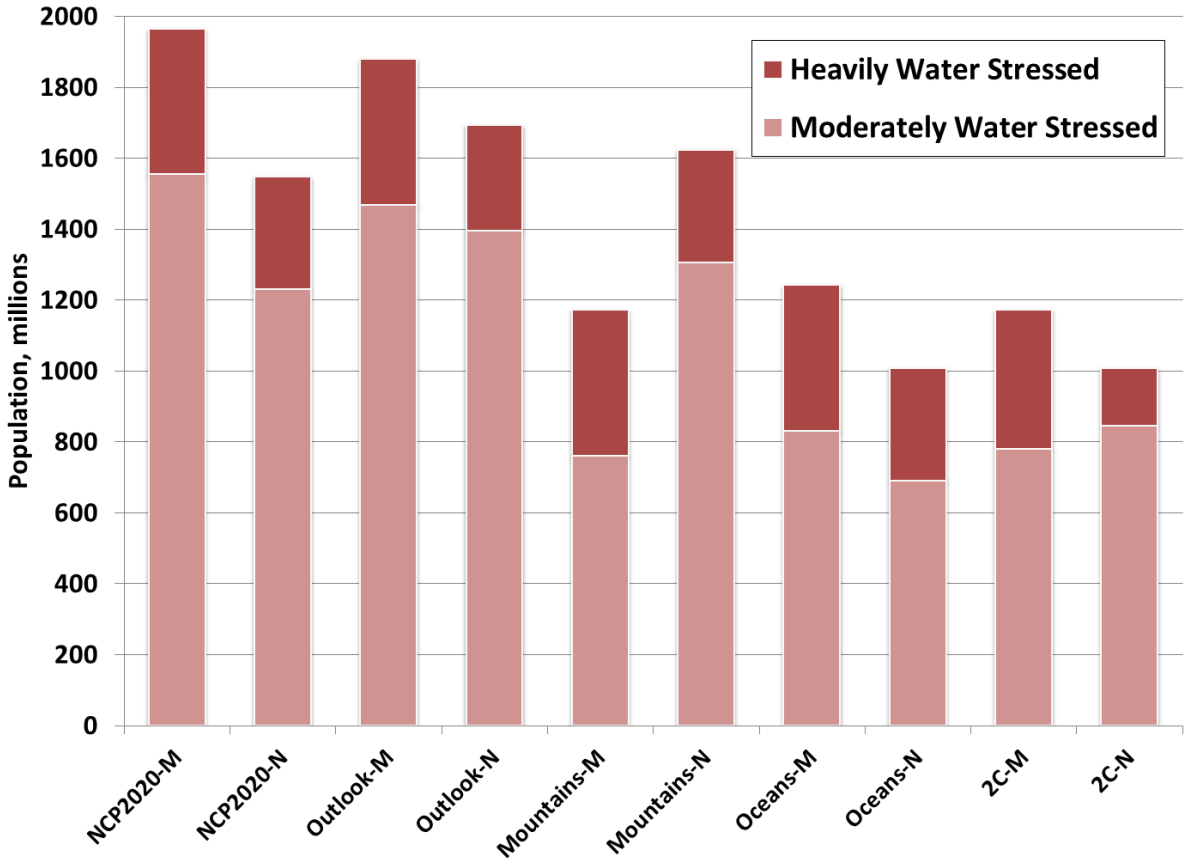

Figure 21. Bar plots denote the changes in global population experiencing heavily stressed (i.e. WSI≥0.6) and moderately stressed (i.e. 0.4≤WSI<0.6) conditions through 2070. The estimate is based on WSI values at every basin (or ASR) averaged over the 2051–2070 period and then using the projected population for each ASR at 2050 (global population is expected to be 9.5 billion). These population changes by 2070 are based against the values calculated at 2020, which indicate that for a global population of 7.5 billion people, approximately 2 billion people are at least living under moderately water-stressed conditions. For each of the scenarios shown, the results for the "M" and "N" climate patterns are given.

6. AIR QUALITY IMPACTS

We used the GEOS-Chem 3-D chemical transport model to predict ground level fine particulate matter ($PM_{2.5}$) concentrations. Concentrations are reported as annual averages, which is common for health standards. GEOS-Chem is widely used to simulate atmospheric pollution formation and transport. Our base case simulation used reanalysis meteorology and anthropogenic emissions for 2010. We projected non-agricultural anthropogenic emissions in ten-year intervals out to 2100 using the projections from the MIT IGSM. In all simulations, meteorological fields from 2010 were used, thus isolating the air quality impact of anthropogenic emissions changes. Biomass burning and biogenic emissions were left constant at 2010 levels. The horizontal grid cell resolution was 2 × 2.5 degrees.

Figure 22 (panel A) shows how annual average $PM_{2.5}$ concentrations evolve in four emissions scenarios, using China as an example. Concentrations in 2010 are 53.8 $\mu g/m^3$; by 2100 values range from 42.9 $\mu g/m^3$ in the *2°C* scenario to 78.9 $\mu g/m^3$ in the *Outlook* scenario. Population-weighted concentrations are also provided in Figure 22 (panel B); these values are a better indicator of exposure to $PM_{2.5}$ in China because of the very heterogeneous spatial distributions of atmospheric pollution and population (most people live in the East). By 2100, *Outlook*, *Mountains*, and *Oceans* scenarios have notably larger population-weighted concentrations (up to 125.4 $\mu g/m^3$ in *Outlook*), while the *2°C* scenario is slightly lower (42.5 $\mu g/m^3$). The US EPA National Ambient Air Quality Standard for annual average $PM_{2.5}$ is 12 $\mu g/m^3$ and the World Health Organization has set their limit at 10 $\mu g/m^3$.

Annual average and population-weighted $PM_{2.5}$ concentrations for India are provided in **Figure 23**. Unlike in Figure 22, the two plots are very similar, which reflects the homogenous spatial distributions of $PM_{2.5}$ and population. In 2010, population-weighted concentrations are 30.2 $\mu g/m^3$. By 2100, the population-weighted concentrations in *Outlook*, *Oceans*, *Mountains*, and *2°C* scenarios are 92.9 $\mu g/m^3$, 45.5 $\mu g/m^3$, 40.9 $\mu g/m^3$, and 21.4 $\mu g/m^3$.

Spatial distributions of 2010 $PM_{2.5}$ concentrations are shown in **Figure 24** (in 2010 these are the same in all scenarios). The left hand figure includes windblown dust, and the figure on the right excludes dust from the calculation to provide a better picture of the anthropogenic contribution to $PM_{2.5}$. (Not all non-dust $PM_{2.5}$ is anthropogenic, but removing dust eliminates a large natural source of $PM_{2.5}$ in China.)

Concentration differences across the scenarios are due to changes in anthropogenic emissions. Windblown dust is identical in all scenarios. Ignoring dust provides a better comparison of the anthropogenic emissions impact for each scenario, which is represented in **Figure 25**. The *Outlook* scenario clearly has larger concentrations in China and India, with maximum grid cell concentrations reaching 172.0 $\mu g/m^3$ in China and 161.4 $\mu g/m^3$ in India. The *Mountains*, *Oceans*, and *2°C* scenarios have lower concentrations relative to *Outlook* in 2100 (Figure 25).

It is worth to note that in this study we focus on the scenarios of GHG mitigation and the figures in this section reflect the changes in $PM_{2.5}$ that are driven by climate policies and the resulting changes in energy technology mix and economic development. Numerous studies explore air quality co-benefits of GHG mitigation, by recognizing that conventional air

pollutants and GHGs are co-generated by fossil-fuel combustion (Nemet *et al.*, 2010; Nam *et al.*, 2014). Additional policies that directly focus on reducing air pollution (e.g., state-of-the-art filters to coal power stations, emission standards for vehicles, etc.) would result in lower $PM_{2.5}$ concentrations than reported here. The exact values will depend on available technologies and stringency of air pollution regulation.

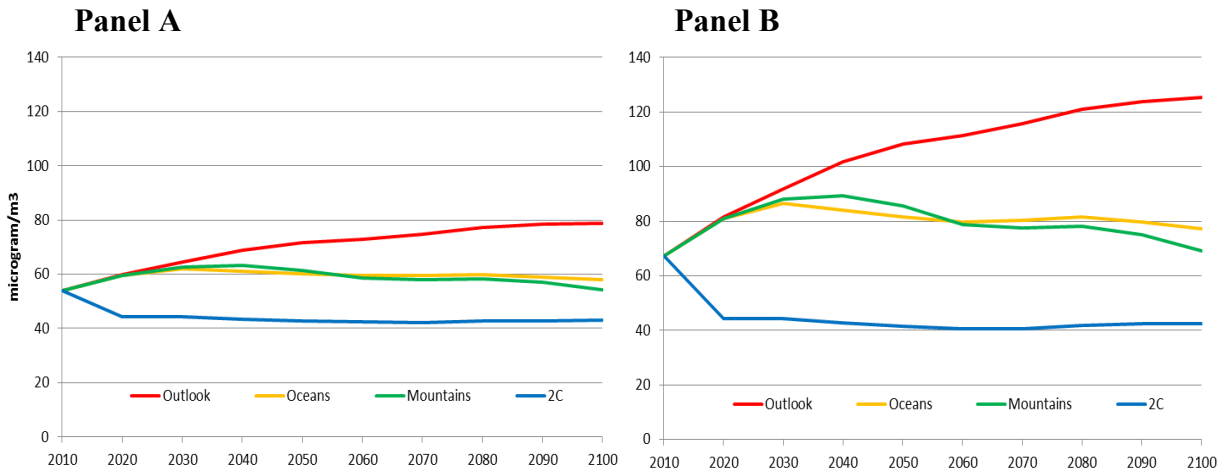

Figure 22. Annual average (Panel A) and population-weighted annual average (Panel B) $PM_{2.5}$ concentrations in China.

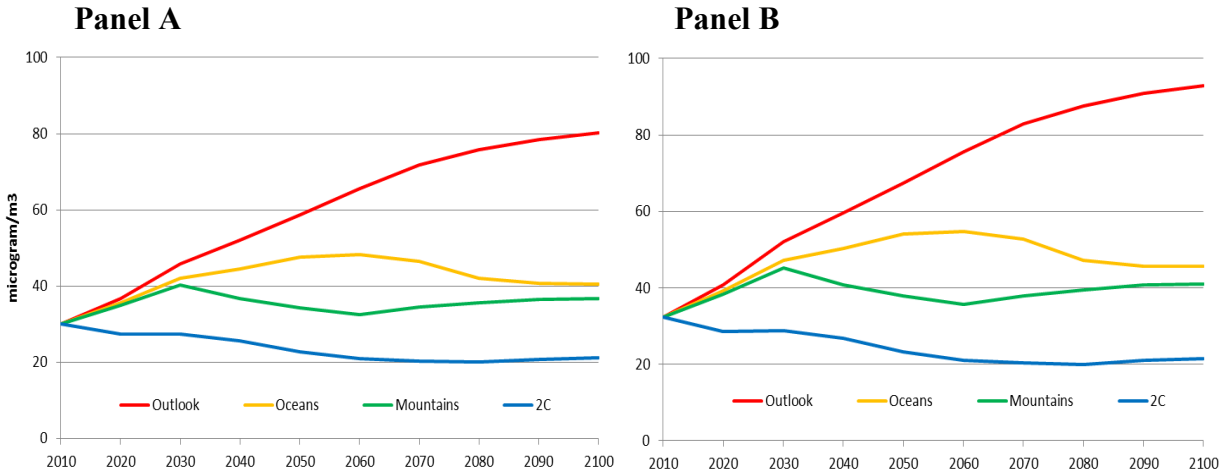

Figure 23. Annual average (Panel A) and population-weighted annual average (Panel B) $PM_{2.5}$ concentrations in India.

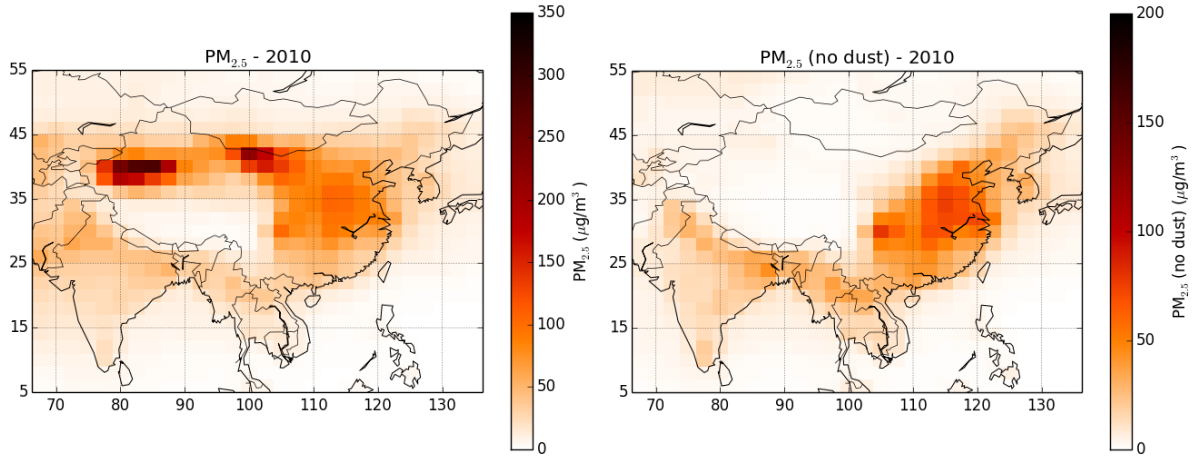

Figure 24. Annual average $PM_{2.5}$ concentrations in 2010 with (left) and without (right) wind-blown dust for all scenarios. Note the different scales.

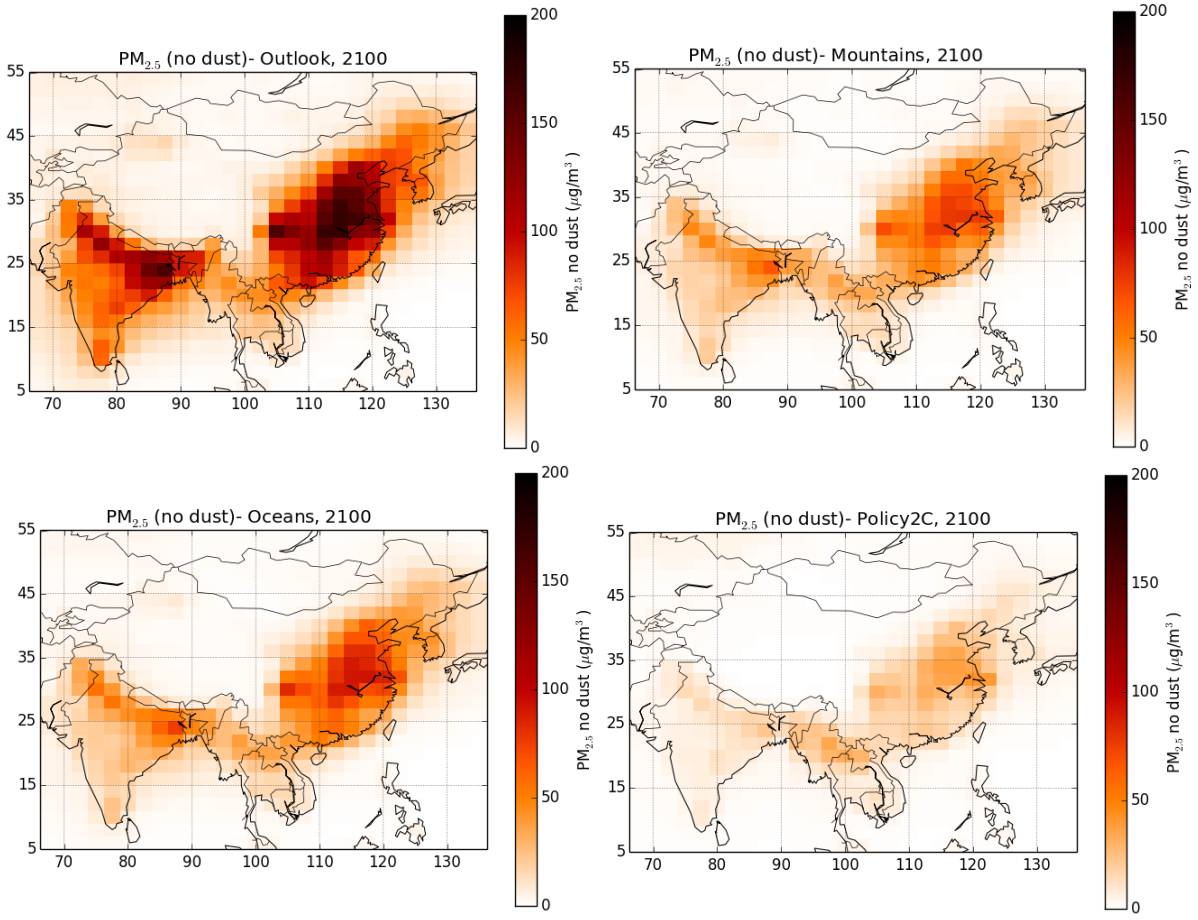

Figure 25. Annual average $PM_{2.5}$ concentrations in 2100 without windblown dust in four scenarios.

7. AGRICULTURAL YIELD CHANGES

To estimate changes in agriculture yields we use the terrestrial ecosystems model (TEM) component of the IGSM, which is a process-based model that describes the carbon, nitrogen and water dynamics of plants and soils for terrestrial ecosystems over the globe (Felzer *et al.*, 2007; Kicklighter *et al.*, 2012). The TEM uses spatially referenced information on climate, elevation, soils and vegetation as well as soil- and vegetation-specific parameters to make estimates of important carbon, nitrogen and water fluxes and pool sizes of terrestrial ecosystems. The TEM has a 1-month time step and a 0.5 × 0.5 degree latitude/longitude spatial resolution. In this study, the TEM model uses the land-use changes projected by the EPPA model along with atmospheric carbon dioxide (CO_2) and ozone (O_3) concentrations and climate variables (temperature, precipitation) from the MESM model to compute net land carbon fluxes.

Initial crop areas are represented in **Figure 26**, where crop land areas (km^2) in the year 2000 are given in in each of the 67,420 grid cells. Land area distribution is based on the Hurtt *et al.* (2006) dataset. Based on latitude, the area of the grid cells varies. The area of grid cells that are close to the equator is on the order of 3,000 km^2. Figure 26 shows that crops occupy the majority of the grid cell areas in parts of South Asia and South-East Asia and North America.

The EPPA model uses climate variables from the MESM model and net primary productivity (NPP) estimates from TEM to predict changes in the land use in each grid cell. The resulting changes from 2000 to 2100 for the *Oceans* and *Mountains* scenarios are provided in **Figures 27 and 28**. In both scenarios, changes in temperature, precipitation, ozone, and land and agricultural prices, lead to substantial changes in the crop areas. For example, parts of Africa and Latin America see a substantial increase in crop areas, mostly due to relatively low land rents and higher precipitation. At the same time, in parts of Europe, North America and South-East Asia crop areas are projected to decrease between 2000 and 2100 due to higher land rents, ozone damages and competition from other land uses.

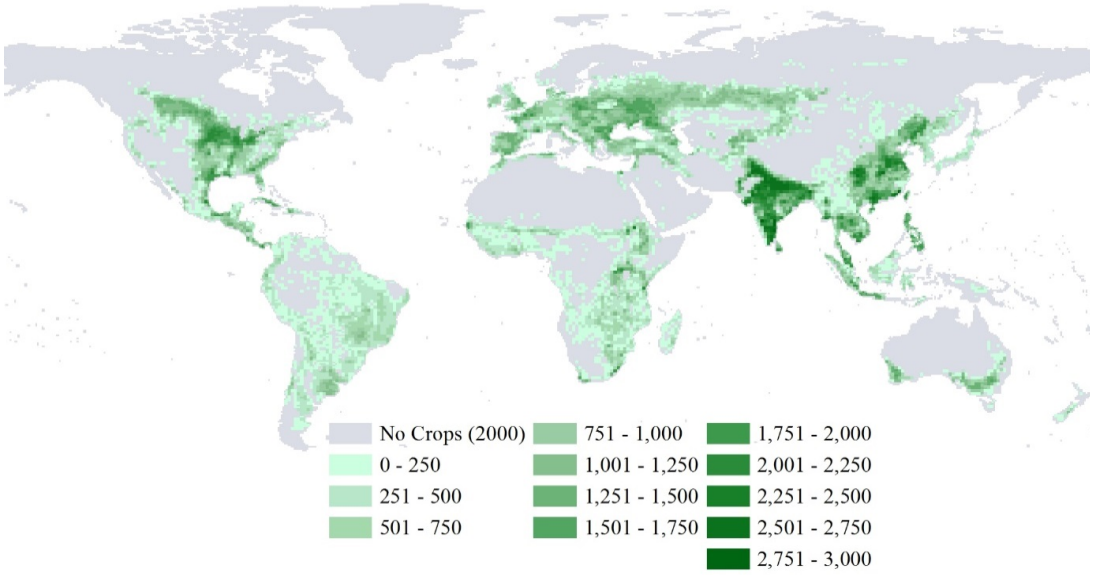

Figure 26. Year 2000 cropland area (km^2) in grid cells.

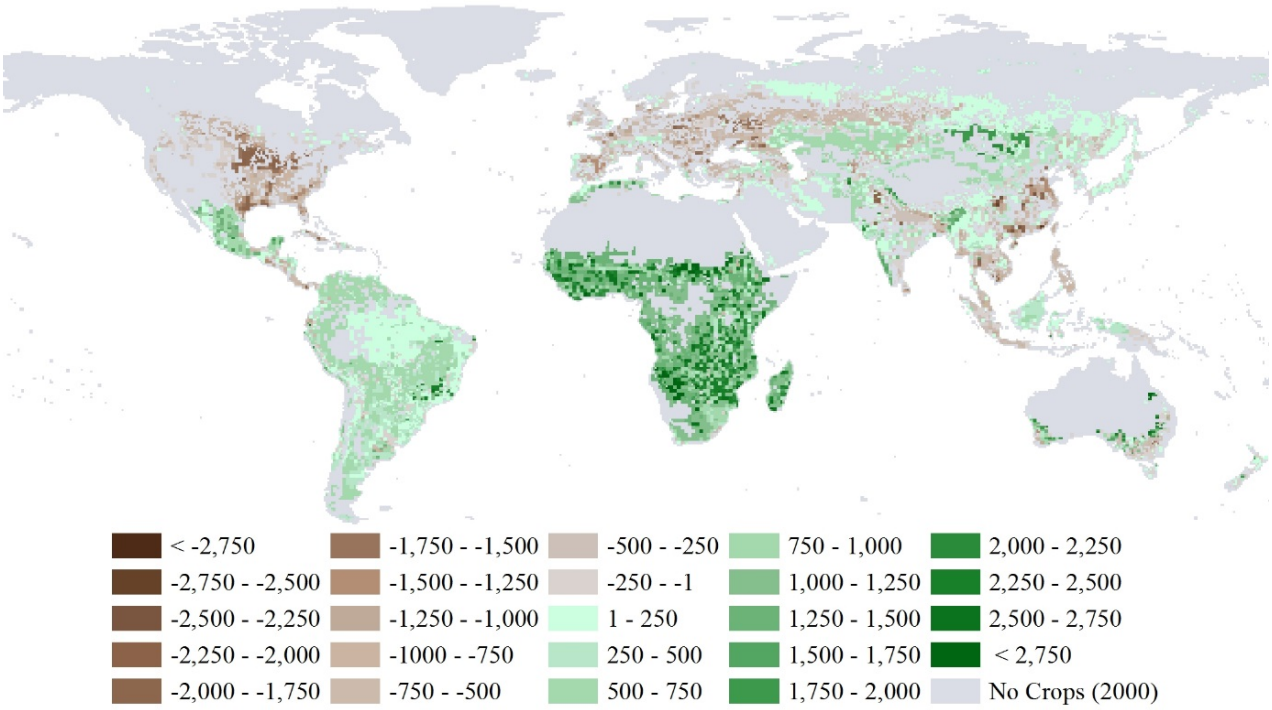

Figure 27. Change in cropland areas (km^2) between 2000 and 2100 in the *Mountains* Scenario.

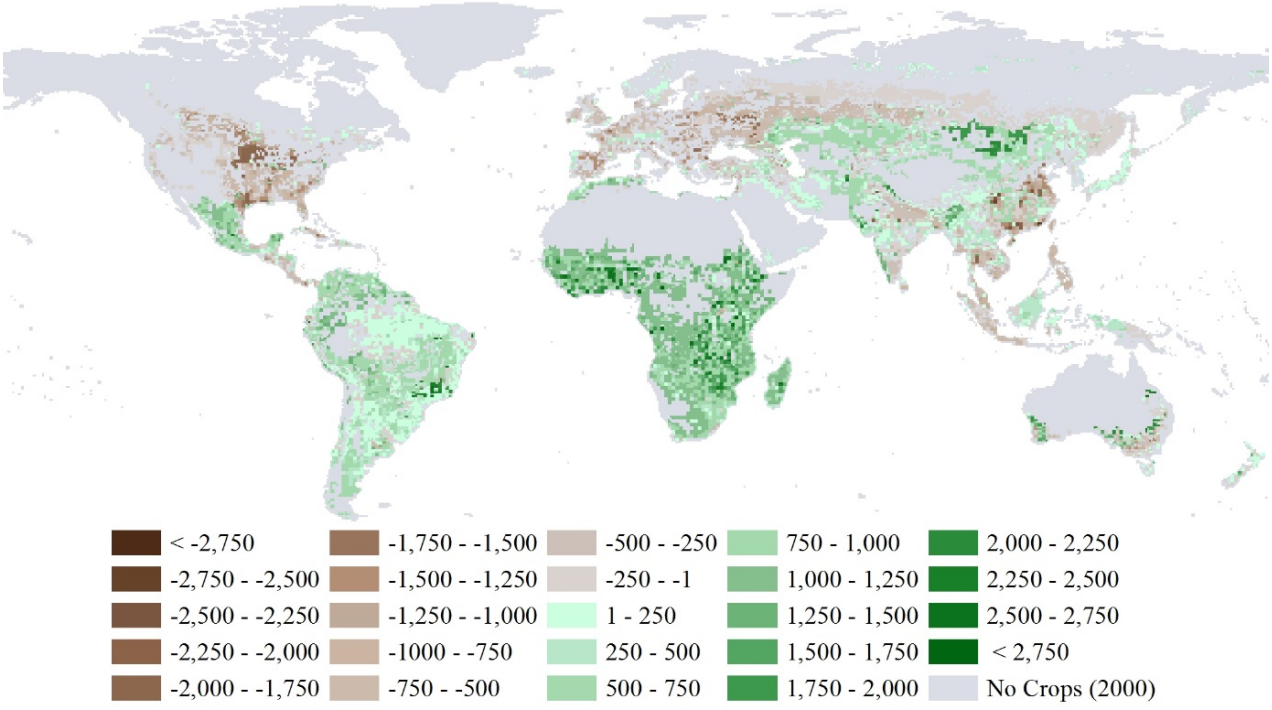

Figure 28. Change in cropland areas (km^2) between 2000 and 2100 in the *Oceans* Scenario.

To assess the yield effects, net primary productivity (NPP) is used, which is a measure of organic carbon added to the vegetation. Vegetation sequesters carbon by atmospheric CO_2 uptake through photosynthesis (gross primary productivity, GPP) and returns carbon to the atmosphere through autotrophic respiration (R_A). NPP = GPP – R_A is then the annual net carbon uptake by vegetation (kgC/year; Felzer *et al.*, 2004). Estimates from the TEM model for NPP in the year 2000 in kilograms of carbon for each grid cell are provided in **Figure 29**. Current land use patterns and climate conditions result in higher NPP in Central America, Sub-Saharan Africa and South-East Asia. Portions of North America, Europe, Asia, Australia and New Zealand also contain cells with substantial NPP values. Substantial portions of Northern America, Northern Eurasia, Central Asia, the Middle East and Australia have grid cell with low NPP (represented by a lighter green color).

Changes in annual NPP between 2000 and 2100 for the *Mountains* scenario are provided in **Figure 30**. **Figure 31** shows the 2000–2100 NPP changes for the *Oceans* scenario. Brown colors represent the areas with a reduction in annual NPP. These reductions are projected mostly in parts of North America, Europe and South-East Asia due to ozone damage from increased air

pollution and precipitation decrease. Africa and South America show mostly NPP increases, which is driven by the projected increases in precipitation in these parts of the world. A notable difference between the *Mountains* and *Oceans* scenarios is in the central parts of South America and some parts of Sub-Saharan Africa. In the TEM model, NPPs are negatively affected when average monthly temperatures are above 33°C. The *Oceans* scenario in 2100 results in the higher temperature that contributes to the NPP losses in these areas. Both scenarios lead to an increase in NPP in the majority of grid cells.

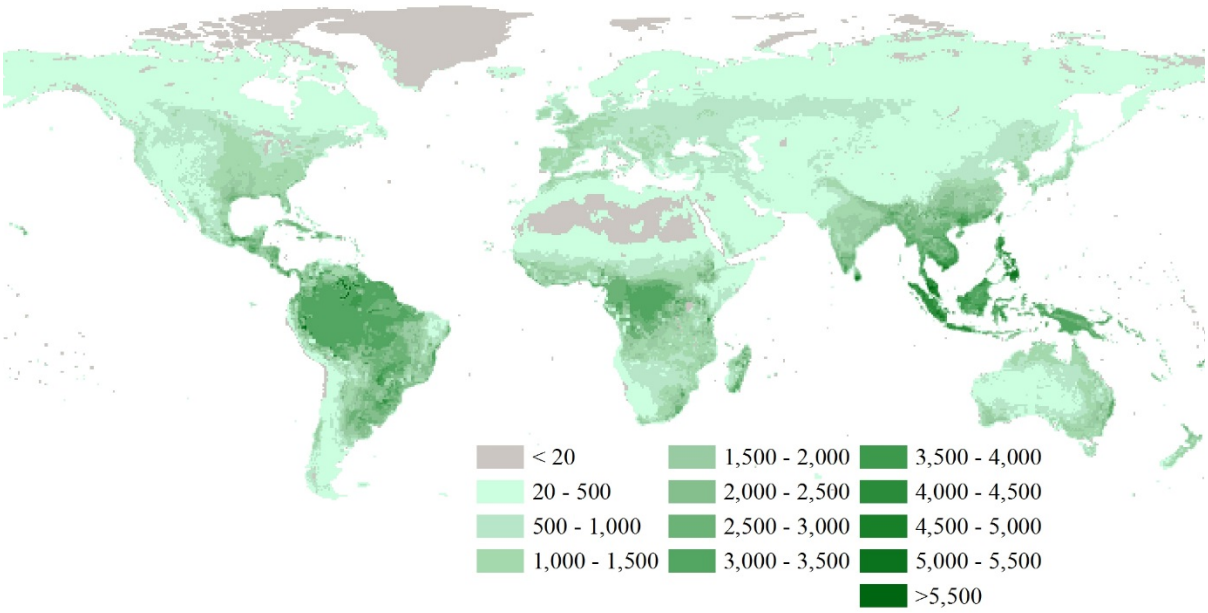

Figure 29. Net primary productivity (NPP) in 2000 (kgC/year).

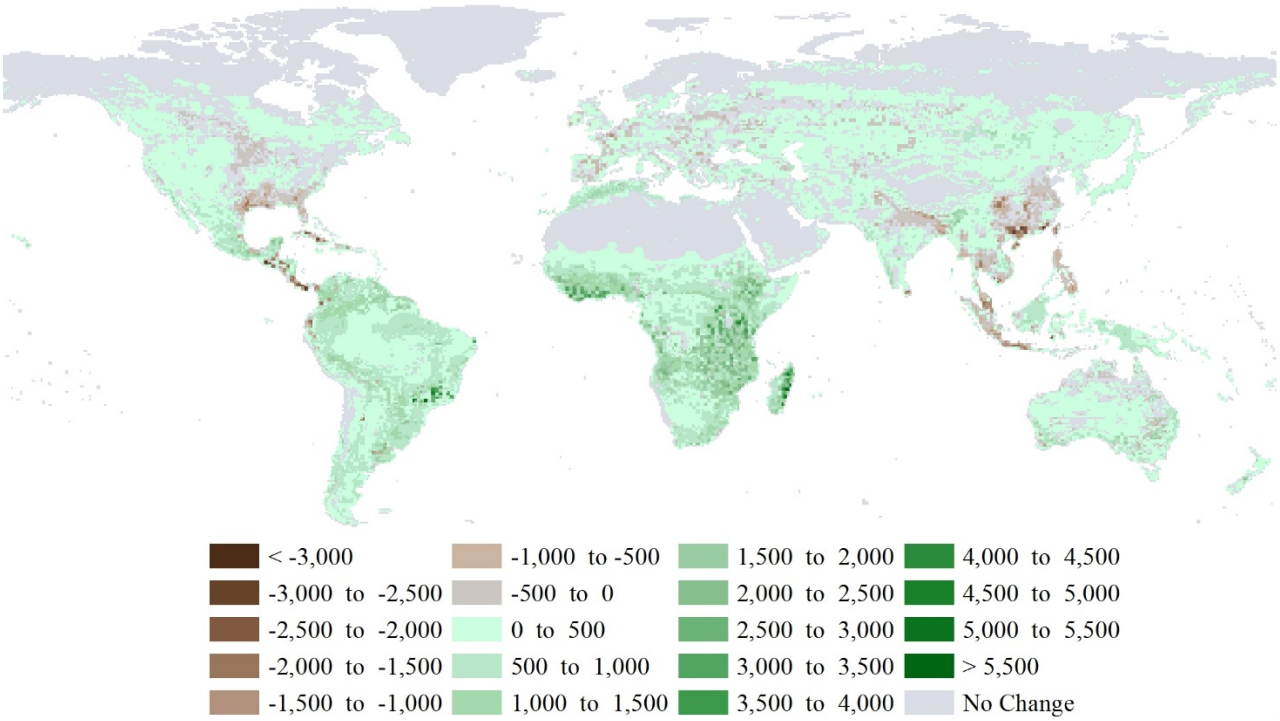

Figure 30. Change in NPP between 2000 and 2100 in the *Mountains* Scenario (kgC/year).

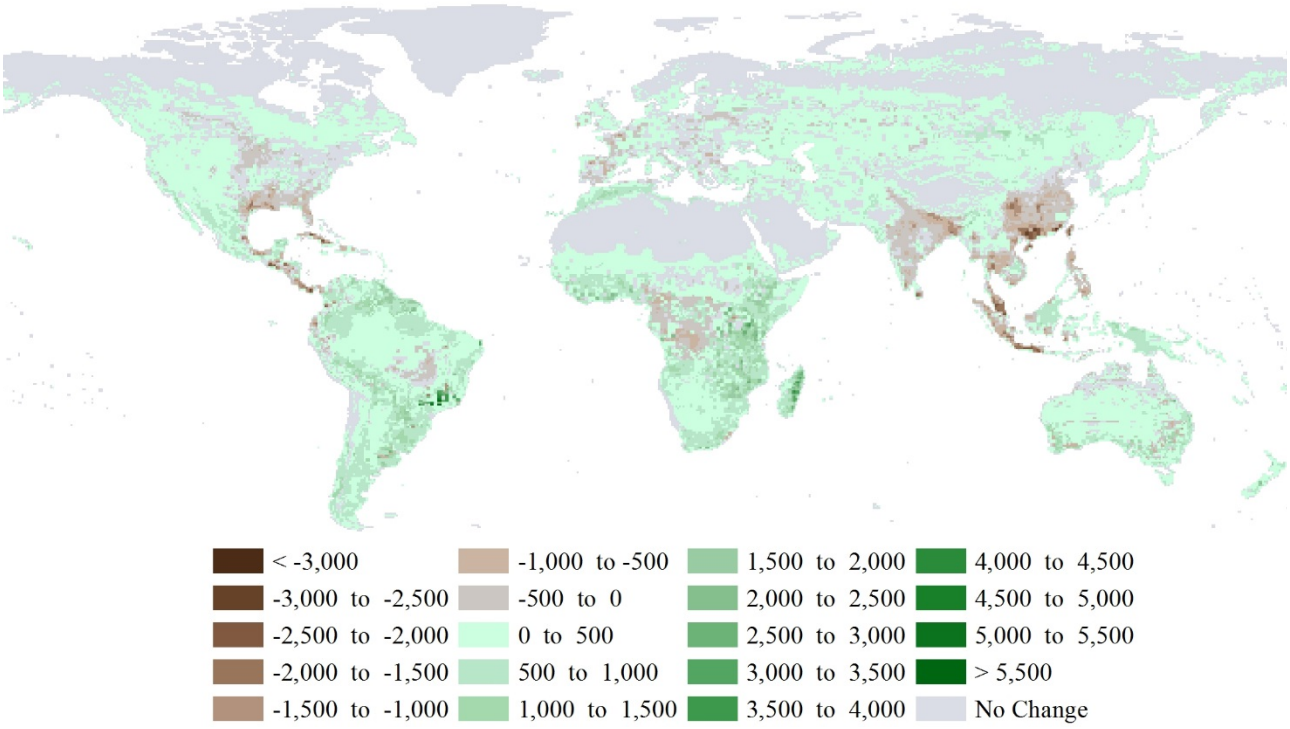

Figure 31. Change in NPP between 2000 and 2100 in the *Oceans* Scenario (kgC/year).

Yields on cropland are taken from TEM estimates of changes in yield for a "generic" C3 crop (Felzer *et al.*, 2004). Information for crop yields for 2000 is provided in **Figure 32**. As with NPP, crop yields are measured as annual additional organic carbon. South Asia, South-East Asia and midlands of North America have grid cells with the largest crop yields in 2000.

Changes in crop yields from 2000 to 2100 are provided in **Figure 33** for the *Mountains* scenario and in **Figure 34** for the *Oceans* scenario. Similar to the figures that show changes in NPP, brown colors represent the areas with a reduction in crop yields, while green colors depict the areas with an increase in crop yields. Negative changes are projected in parts of North America, Europe, South Asia and South-East Asia, mostly driven by changes in ozone damage, and temperature and precipitation changes. Africa and South America are mostly positively affected, which is driven by the projected increases in precipitation in these parts of the world. As with NPP, a notable difference between the *Mountains* and *Oceans* scenarios is in the central parts of Central America, where in the *Oceans* scenario crop yields are negatively affected when average monthly temperatures are above 33°C.

Multiple climate and environmental changes will have consequences for global vegetation. These effects vary by region. The largest negative effects on annual NPP and crop yields occur in the areas exposed to increased ozone concentrations and reduced precipitation. The results for the *Oceans* and *Mountains* scenarios reveal that despite the CO_2 fertilization effect (an increase in NPP and yields due to higher CO_2 concentrations), mid- and high-latitude areas (parts of Eurasia and North America) see substantial negative yield effects. Yet the largest negative yield effects are in South Asia and South-East Asia, which are impacted by higher ozone concentrations, lower

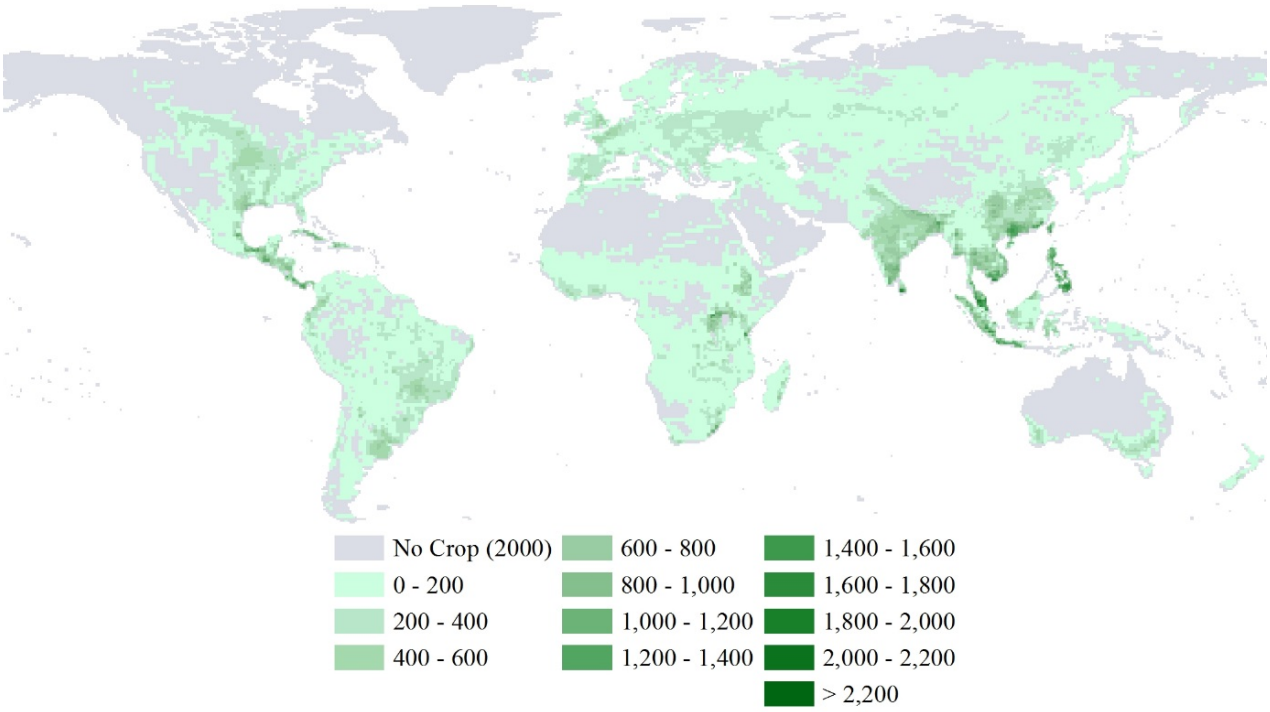

Figure 32. Crop yield (kgC/year) in 2000 per grid cell.

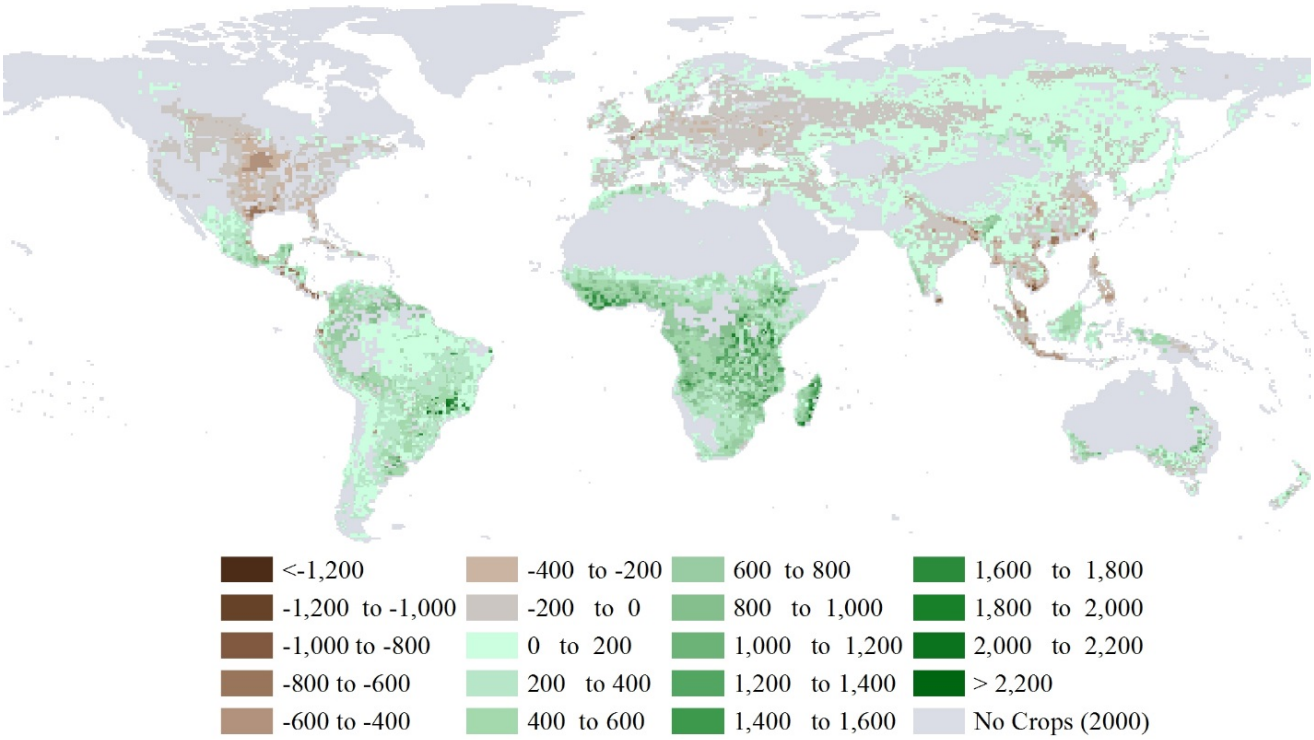

Figure 33. Change in crop yield (kgC/year) between 2000 and 2100 in the *Mountains* Scenario.

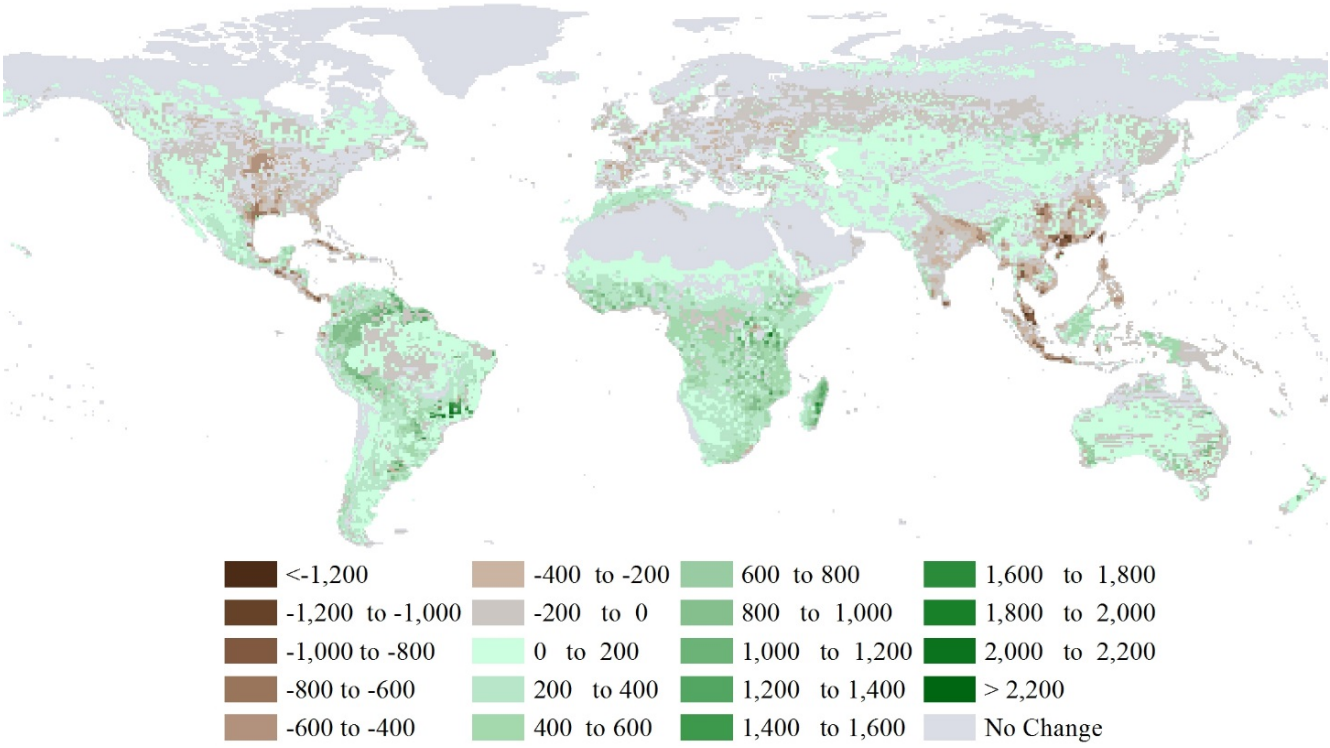

Figure 34. Change in crop yield (kgC/year) between 2000 and 2100 in the *Oceans* Scenario.

precipitation and increased occurrence of months with average temperatures higher than 33°C. Parts of Sub-Saharan Africa and South America are positively impacted by the CO_2 fertilization effect and increased precipitation. There are some caveats to the results presented above. As in our previous studies (e.g., Reilly *et al.*, 2007; Kicklighter *et al.*, 2012), TEM grows the "generic" crop as soon as the weather is suitable and if the season is lengthened TEM automatically grows additional crops. In some subtropical regions, winter cropping improves even if summer cropping fails. The "generic" TEM crop is a C3 crop (i.e., grains, beans and vegetables) that responds relatively strongly to CO_2 fertilization. In reality, agriculture includes C4 crops (i.e., maize and sorghum), which are less responsive to CO_2 concentration, and so the average response including C4 crops is likely to be lower than we estimate. The TEM estimates assume an optimum nitrogen fertilization of crops, so that CO_2 fertilization is not nitrogen-limited as it would be for natural vegetation or under conditions where fertilizer application is not optimal. Thus, neither spatial nor temporal variations in the amount, timing and the effectiveness of fertilizer applications have been considered, which may also contribute to the positive effect. Additionally, the TEM simulations do not consider the influence of irrigation so that crop productivity may be underestimated in arid regions. TEM models vegetation on a monthly basis for a generic crop and does not account for daily or weekly temperature spikes. Crop yield for specific crops can be severely affected by short periods of heat or drought during key developmental phases. Despite these limitations, TEM results are relevant as they can be considered to represent a case where crop breeding or changes in crop type enable adaption that overcomes these limitations as climate changes. With these caveats, the results presented above should be treated as informing general regional trends in crop yield effects rather than as predictions for each particular grid cell.

8. CONCLUSIONS

Assessing climate change impacts is a challenging task. The world has not experienced the current greenhouse gas (GHG) concentrations over the past 650,000 years as recorded in ice cores. In this study we considered three types scenarios: a) projections of the future based on an assessment of current climate policies and pledges and removal of these after 2020; b) exploratory scenarios with differing energy system development; and c) a target-driven pathway to reach 2°C stabilization by 2100. These scenarios show that significant policy measures are needed to stabilize temperatures and climate impacts. They also illustrate the scale of the needed transformation in the energy and other sectors in the economy. Uncontrolled emissions are projected to increase the global mean surface temperature by more than 4°C by 2100 in comparison to pre-industrial levels. Our study shows that the COP-21 agreement in Paris will succeed in a useful lowering of the trend of global GHG emissions. It will not, however, reduce global emissions to a trajectory to 2°C or even 3°C stabilization by 2100. Exploratory and target-driven scenarios show that a substantial additional de-carbonization, especially in the second part of the 21st century, is needed to achieve more tolerable climate goals.

The two Shell scenarios explore a plausible development of how climate change might steadily move up in the public and political agendas following the COP-21 meeting in Paris. In

this report we evaluated a wider range of scenarios: No policy after Paris (*NCP2020*), policies likely agreed upon in Paris (*Outlook*), rising response to climate concern (*Oceans* and *Mountains*), and the aspirational case (*2°C*). The Paris Agreement will not succeed in reaching the goal of 2°C limit, and without further policy measures it is projected to result in a 3.5°C increase in global temperature in 2100 relative to pre-industrial levels. *Mountains* and *Oceans* exhibit a substantial movement towards temperature stabilization, as they result in only 2.4–2.7°C increases by 2100. In addition to a substantial shift to renewable energy and deployment of carbon capture and storage (CCS), availability of a negative emission technology (e.g. biomass with CCS) and policies on non-CO_2, GHGs are valuable components of potential climate stabilization pathways.

Many researchers are cautious about reducing all impacts to a dollar value because very little is known about damage functions, there is no theory to guide their improvement, and in many cases arbitrary functional forms and corresponding parameter values are chosen (Pindyck, 2013). In contrast to the approach of assessing climate impacts by estimating the so called damage function, i.e., the relationship between an increase in temperature and GDP (or the growth rate of GDP), here we focused on understanding the chain of physical changes – global and regional temperature, precipitation, ocean acidification, air pollution, water availability and agricultural yields. Our results show that the projected climate impacts vary dramatically across the globe. The use of different climate patterns shows that we have to treat the exact numbers or specific forecasts extremely carefully. Current knowledge is still far from allowing us to make long-term specific projections for a particular area. However, some general observations about the prevailing trends can be made. Our analysis shows that more stringent emission reduction scenarios (*Oceans*, *Mountains*, *2°C*) are successful in mitigating a large portion of water stress impacts and air pollution damages. They also cap the ocean acidity increase, while agricultural yields are still strongly affected. These projections show a significant value of policies that may not end up in 2°C stabilization but fall substantially close to that target by the end of the century.

Acknowledgements

The paper benefitted from comments from John Reilly. The MIT Joint Program on the Science and Policy of Global Change is supported by the U.S. Department of Energy, Office of Science under grants DE-FG02-94ER61937, DE-FG02-08ER64597, DE-FG02-93ER61677, DE-SC0003906, DE-SC0007114, XEU-0-9920-01; the U.S. Department of Energy, Oak Ridge National Laboratory under Subcontract 4000109855; the U.S. Environmental Protection Agency under grants XA-83240101, PIv83412601-0, RD-83427901-0, XA-83505101-0, XA-83600001-1, and subcontract UTA12-000624; the U.S. National Science Foundation under grants AGS-0944121, EFRI-0835414, IIS-1028163, ECCSv1128147, ARC-1203526, EF-1137306, AGS-1216707, and SES-0825915; the U.S. National Aeronautics and Space Administration under grants NNX06AC30A, NNX07AI49G, NNX11AN72G and Sub Agreement No. 08-SFWS-209365.MIT; the U.S. Federal Aviation Administration under grants 06-C-NE-MIT, 09-C-NE-MIT, Agmt. No. 4103-30368; the U.S. Department of Transportation under grant DTRT57-10-C-10015; the Electric Power Research Institute under grant EP-P32616/C15124, EP-P8154/C4106; the U.S. Department of Agriculture under grant 58-6000-2-0099, 58-0111-9-001; and a consortium of industrial and foundation sponsors (for the complete list see: globalchange.mit.edu/sponsors/all). Shell participated actively in this study, supplying all the background data behind their scenarios. MIT remain responsible for

all analysis and conclusions. Shell provided a gift of USD 250,000 to the MIT Joint Program, to defray costs related to this research. Martin Haigh represents the Scenarios Team at Shell International Ltd. The paper also benefited from comments from David Hone.

9. REFERENCES

Bindoff, N., P. Scott, K. AchutaRao, M. Allen, N. Gillett, D. Gutzler, K. Hansingo, G. Hegerl, Y. Hu, S. Jain, I. Mokhov, J. Overland, J. Perlwitz, R. Sebbari and X. Zhang, 2013: *Detection and Attribution of Climate Change: From Global to Regional*. In: Climate Change 2013: The Physical Science Basis. Contribution of Working Group 1 to the Fifth Assessment Report of the Intergovernmental Panel on Climate Change [Stocker, T.F. et al (eds.)]. Cambridge University Press, Cambridge, United Kingdom and New York, NY, USA.

Blanc E., K. Strzepek, A. Schlosser, A. Gueneau, C. Fant, S. Rausch and J. Reilly, 2014: Modeling U.S. water resources under climate change. *Earth's Future*, 2(4) 197–224.

BP 2015: *Statistical Review of World Energy*. BP plc, London, UK.

CDIAC [Carbon Dioxide Information Analysis Center], 2014: *Recent Greenhouse Gas Concentrations*. Oak Ridge National Laboratory, Oak Ridge, TN (http://cdiac.ornl.gov/pns/current_ghg.html).

Chen, Y.-H.H., S. Paltsev, J. Reilly, J. Morris and M. Babiker, 2015: The MIT EPPA6 Model: Economic Growth, Energy Use, and Food Consumption. MIT Joint Program on the Science and Policy of Global Change *Report 278*, Cambridge, MA (http://globalchange.mit.edu/files/document/MITJPSPGC_Rpt278.pdf).

Dutkiewicz S., A. Sokolov, J. Scott and P. Stone, 2005: A three-dimensional ocean-sea-ice-carbon cycle model and its coupling to a two-dimensional atmospheric model: uses in climate change studies. MIT Joint Program on the Science and Policy of Global Change *Report 122,* Cambridge, MA (http://globalchange.mit.edu/files/document/MITJPSPGC_Rpt122.pdf).

EC [European Commission], 2014: *Climate Impacts in Europe: The JRC PESETA II Project*. Publications Office of European Union, Luxemburg.

EPA [Environmental Protection Agency], 2015: *Climate Change in the United States: Benefits of Global Action*. US Environmental Protection Agency, Washington, DC (http://www2.epa.gov/cira).

Fant, C., C.A. Schlosser, X. Gao, K. Strzepek and J. Reilly, 2014: A Framework for Analysis of the Uncertainty of Socioeconomic Growth and Climate Change on the Risk of Water Stress: a Case Study in Asia. MIT Joint Program on the Science and Policy of Global Change *Report 269*, Cambridge, MA.

Felzer, B., D. Kicklighter, J. Melillo, C. Wang, Q. Zhuang and R. Prinn, 2004: Effects of ozone on net primary production and carbon sequestration in the conterminous United States using a biogeochemistry model. *Tellus B* **56**, 230–248.

Felzer, B. S., T. Cronin, J. M. Reilly, J. M. Melillo and X. Wang. 2007: Impacts of ozone on trees and crops. *Comptes Rendus Geoscience* **339**: 784–798.

Fettweis X., B. Franco, M. Tedesco, J. van Angelen, J. Lenaerts, M. van den Broeke and H. Gallee, 2013: Estimating the Greenland ice sheet surface mass balance contribution to future sea level rise using the regional atmospheric climate model MAR. *The Cryosphere* **7**, 469–489.

Hurtt, G., S. Frolking, M. Fearon, B. Moore, E. Shevliakova, S. Malyshev, S. Pacala and R. Houghton, 2006: The underpinnings of land-use history: Three centuries of global gridded land-use transitions, wood-harvest activity, and resulting secondary lands. *Global Change Biology* **12**, 1208–1229.

IEA [International Energy Agency], 2014: *World Energy Outlook*. IEA/OECD, Paris, France.

IMF [International Monetary Fund], 2015: *World Economic Outlook*. IMF, Washington, DC.

IPCC [Intergovernmental Panel for Climate Change], 2014: *Climate Change 2014 Synthesis Report, Summary for Policymakers* (http://www.ipcc.ch/pdf/assessment-report/ar5/syr/AR5_SYR_FINAL_SPM.pdf).

Jacoby H. and Y.-H. Chen, 2014: Expectations for a New Climate Agreement. MIT Joint Program on the Science and Policy of Global Change *Report 264*, Cambridge, MA (http://globalchange.mit.edu/research/publications/2835).

Jacoby H. and Y.-H. Chen, 2015: Launching a New Climate Regime. MIT Joint Program on the Science and Policy of Global Change *Report 286*, Cambridge, MA (http://globalchange.mit.edu/research/publications/2925).

Kicklighter, D., A. Gurgel, J. Melillo, J. Reilly and S. Paltsev, 2012: Potential Direct and Indirect Effects of Global Cellulosic Biofuel Production on Greenhouse Gas Fluxes from Future Land-use Change. MIT Joint Program on the Science and Policy of Global Change *Report 210*, Cambridge, MA (http://globalchange.mit.edu/files/document/MITJPSPGC_Rpt210.pdf).

MIT Joint Program, 2015: Energy and Climate Outlook: Perspectives from 2015, MIT Joint Program on the Science and Policy of Global Change. Cambridge, MA (http://globalchange.mit.edu/Outlook2015).

Monier, E., J. Scott, A. Sokolov, C. Forest and A. Schlosser, 2013: An integrated assessment modeling framework for uncertainty studies in global and regional climate change: the MIT IGSM-CAM (version 1.0). *Geosci. Model Dev.* **6**, 2063–2085.

Nam, K-M., C. Waugh, S. Paltsev, J. Reilly and V. Karplus, 2014: Synergy between Pollution and Carbon Emissions Control: Comparing China and the United States. *Energy Economics* **46**, 186–201.

Nemet, G., T. Holloway and P. Meier, 2010: Implications of Incorporating Air-quality Co-benefits into Climate Change Policymaking. *Environmental Research Letters* **5**, 014007.

Paltsev, S., E. Monier, J. Scott, A. Sokolov and J. Reilly, 2015: Integrated Economic and Climate Projections for Impact Assessment. *Climatic Change* **131**(1), 21–33.

Pindyck, R., 2013: Climate Change Policy: What Do the Models Tell Us? *Journal of Economic Literature* **51**(3), 860–872.

Prinn, R., S. Paltsev, A. Sokolov, M. Sarofim, J. Reilly and H. Jacoby, 2011: Scenarios with MIT Integrated Global Systems Model: Significant Global Warming Regardless of Different Approaches. *Climatic Change* **104**(3–4), 515–537.

Prinn, R. 2013: Development and Application of Earth System Models. *Proceedings of the National Academy of Sciences (PNAS)* **110**, 3673–3680.

Reilly, J., S. Paltsev, B. Felzer, X. Wang, D. Kicklighter, J. Melillo, R. Prinn, M. Sarofim and C. Wang, 2007: Global Economic Effects of Changes in Crops, Pasture, and Forests due to Changing Climate, Carbon Dioxide, and Ozone. *Energy Policy* **35**(11), 5370–5383.

Reilly, J., S. Paltsev, K. Strzepek, N.E. Selin, Y. Cai, K.-M. Nam, E. Monier, S. Dutkiewicz, J. Scott, M. Webster and A. Sokolov, 2013: Valuing climate impacts in integrated assessment models: the MIT IGSM. *Climatic Change* **117**(3), 561–573.

Schlosser, C.A., K. Strzepek, X. Gao, A. Gueneau, C. Fant, S. Paltsev, B. Rasheed, T. Smith-Greico, E. Blanc, H. Jacoby and J. Reilly, 2014: The Future of Global Water Stress: An Integrated Assessment. *Earth's Future* **2**(8), 341–361.

Schlosser, C. A., X. Gao, K. Strzepek, C. Forest, A. Sokolov, S. Awadalla and W. Farmer, 2013: Quantifying the Likelihood of Regional Climate Change: A Hybridized Approach. *Journal of Climate* **26**, 3394–3414.

Shell, 2013: *New Lens Scenarios*. London, UK (http://www.shell.com/global/future-energy/scenarios/new-lens-scenarios.html).

Sokolov A., 2006: Does Model Sensitivity to Changes in CO_2 Provide a Measure of Sensitivity to Other Forcings? *Journal of Climate* **19**, 3294–3306.

Sokolov A., S. Dutkiewicz, P. Stone and J. Scott, 2007: Evaluating the use of ocean models of different complexity in climate change studies. MIT Joint Program for the Science and Policy of Global Change *Report 128*, Cambridge, MA (http://globalchange.mit.edu/files/document/MITJPSPGC_Rpt128.pdf).

Sokolov, A., P. Stone, C. Forest, R. Prinn, M. Sarofim, M. Webster, S. Paltsev, A. Schlosser, D. Kicklighter, S. Dutkiewicz, J. Reilly, C. Wang, B. Felzer and H. Jacoby, 2009: Probabilistic Forecast for 21st Century Climate Based on Uncertainties in Emissions (Without Policy) and Climate Parameters. *Journal of Climate* **22**, 5175–5204.

Sokolov, A., S. Paltsev, H. Chen, M. Haigh and R. Prinn, 2015: Climate Stabilization at 2°C and "Net Zero" Emissions. MIT Joint Program on the Science and Policy of Global Change, Report, Cambridge, MA (forthcoming).

Strzepek, K., A. Schlosser, A. Gueneau, X. Gao, E. Blanc, C. Fant, B. Rasheed and H. Jacoby, 2013: Modeling water resource systems within the framework of the MIT Integrated Global System Model: IGSM-WRS, *Journal of Advances in Modeling Earth Systems* **5**(1): 1–16.

Velicogna, I., T. Sutterley and M. van den Broeke, 2014: Regional acceleration in ice mass loss from Greenland and Antarctica using GRACE time-variable gravity data. *J. Geophys. Res. Space Physics* **41**, 8130–8137.

Wang C., R. Prinn and A. Sokolov, 1998: A global interactive chemistry and climate model: Formulation and testing. *J. Geophys. Res.* **103,** 3399–3418

Yan, Q., H. Wang, O. Johannessen and Z. Zhang, 2014: Greenland ice sheet contribution to future global sea level rise based on CMIP5 models. *Adv. in Atmos. Sci* **31**, 8–16.

REPORT SERIES of the MIT Joint Program on the Science and Policy of Global Change

FOR THE COMPLETE LIST OF JOINT PROGRAM REPORTS: http://globalchange.mit.edu/pubs/all-reports.php

253. **An Analogue Approach to Identify Extreme Precipitation Events: *Evaluation and Application to CMIP5 Climate Models in the United States*.** *Gao et al.* November 2013
254. **The Future of Global Water Stress: *An Integrated Assessment*.** *Schlosser et al.*, January 2014
255. **The Mercury Game: *Evaluating a Negotiation Simulation that Teaches Students about Science–Policy Interactions*.** *Stokes and Selin,* January 2014
256. **The Potential Wind Power Resource in Australia: *A New Perspective*.** *Hallgren et al.,* February 2014
257. **Equity and Emissions Trading in China.** *Zhang et al.,* February 2014
258. **Characterization of the Wind Power Resource in Europe and its Intermittency.** *Cosseron et al.,* March 2014
259. **A Self-Consistent Method to Assess Air Quality Co-Benefits from US Climate Policies.** *Saari et al.,* April 2014
260. **Electricity Generation and Emissions Reduction Decisions under Policy Uncertainty: *A General Equilibrium Analysis*.** *Morris et al.,* April 2014
261. **An Integrated Assessment of China's Wind Energy Potential.** *Zhang et al.,* April 2014
262. **The China-in-Global Energy Model.** *Qi et al.* May 2014
263. **Markets versus Regulation: *The Efficiency and Distributional Impacts of U.S. Climate Policy Proposals*.** *Rausch and Karplus,* May 2014
264. **Expectations for a New Climate Agreement.** *Jacoby and Chen,* August 2014
265. **Coupling the High Complexity Land Surface Model ACASA to the Mesoscale Model WRF.** *Xu et al.,* August 2014
266. **The CO_2 Content of Consumption Across US Regions: *A Multi-Regional Input-Output (MRIO) Approach*.** *Caron et al.,* August 2014
267. **Carbon emissions in China: *How far can new efforts bend the curve?*** *Zhang et al.,* October 2014
268. **Characterization of the Solar Power Resource in Europe and Assessing Benefits of Co-Location with Wind Power Installations.** *Bozonnat and Schlosser,* October 2014
269. **A Framework for Analysis of the Uncertainty of Socioeconomic Growth and Climate Change on the Risk of Water Stress: *a Case Study in Asia*.** *Fant et al.*, November 2014
270. **Interprovincial Migration and the Stringency of Energy Policy in China.** *Luo et al.*, November 2014
271. **International Trade in Natural Gas: *Golden Age of LNG?*** *Du and Paltsev,* November 2014
272. **Advanced Technologies in Energy-Economy Models for Climate Change Assessment.** *Morris et al.,* December 2014
273. **The Contribution of Biomass to Emissions Mitigation under a Global Climate Policy.** *Winchester and Reilly,* January 2015
274. **Modeling regional transportation demand in China and the impacts of a national carbon constraint.** *Kishimoto et al.,* January 2015.
275. **The Impact of Advanced Biofuels on Aviation Emissions and Operations in the U.S.** *Winchester et al.,* February 2015
276. **Specifying Parameters in Computable General Equilibrium Models using Optimal Fingerprint Detection Methods.** *Koesler,* February 2015
277. **Renewables Intermittency: Operational Limits and Implications for Long-Term Energy System Models.** *Delarue and Morris,* March 2015
278. **The MIT EPPA6 Model: Economic Growth, Energy Use, and Food Consumption.** *Chen et al.,* March 2015
279. **Emulating maize yields from global gridded crop models using statistical estimates.** *Blanc and Sultan,* March 2015
280. **Water Body Temperature Model for Assessing Climate Change Impacts on Thermal Cooling.** *Strzepek et al.,* May 2015
281. **Impacts of CO_2 Mandates for New Cars in the European Union.** *Paltsev et al.,* May 2015
282. **Natural Gas Pricing Reform in China: Getting Closer to a Market System?** *Paltsev and Zhang,* July 2015
283. **Global population growth, technology, and Malthusian constraints: *A quantitative growth theoretic perspective*.** *Lanz et al.,* October 2015
284. **Capturing Natural Resource Dynamics in Top-Down Energy-Economic Equilibrium Models.** *Zhang et al.,* October 2015
285. **US Major Crops' Uncertain Climate Change Risks and Greenhouse Gas Mitigation Benefits.** *Sue Wing et al.,* October 2015
286. **Launching a New Climate Regime.** *Jacoby and Chen,* November 2015
287. **Impact of Canopy Representations on Regional Modeling of Evapotranspiration using the WRF-ACASA Coupled Model.** *Xu et al.,* December 2015
288. **The Influence of Gas-to-Liquids and Natural Gas Production Technology Penetration on the Crude Oil-Natural Gas Price Relationship.** *Ramberg et al.*, December 2015
289. **The Impact of Climate Policy on Carbon Capture and Storage Deployment in China.** *Zhang et al.,* December 2015
290. **Modeling Uncertainty in Climate Change: A Multi-Model Comparison.** *Gillingham et al.*, December 2015
291. **Scenarios of Global Change: Integrated Assessment of Climate Impacts.** *Paltsev et al.*, February 2016

Contact the Joint Program Office to request a copy. The Report Series is distributed at no charge.